CHAPTER 6

CLOUDS

6.1 RTE in Cloudy Conditions

Thus far, we have considered the RTE only in a clear sky condition. When we introduce clouds into the radiation field of the atmosphere the problem becomes more complex. The following notes indicate some of the fundamental problems concerning clouds.

If we assume that the fractional cloud cover within the field of view of the satellite radiometer is represented by η and the cloud top pressure by p_o, then the spectral radiance measured by the satellite radiometer at the top of the atmosphere is given by

$$I_\lambda = \eta\, I_\lambda^{cd} + (1 - \eta)\, I_\lambda^{c}$$

where cd denotes cloud and c denotes clear. As before, we can write for the clear radiance

$$I_\lambda^{c} = B_\lambda(T_s)\, \tau_\lambda(p_s) + \int_{p_s}^{o} B_\lambda(T(p))\, d\tau_\lambda \, .$$

The cloud radiance is represented by

$$I_\lambda^{cd} = (1-\varepsilon_\lambda)\, B_\lambda(T_s)\, \tau_\lambda(p_s) + (1-\varepsilon_\lambda) \int_{p_s}^{p_c} B_\lambda(T(p))\, d\tau_\lambda$$

$$+ \varepsilon_\lambda\, B_\lambda(T(p_c))\, \tau_\lambda(p_c) + \int_{p_c}^{o} B_\lambda(T(p))\, d\tau_\lambda$$

where ε_λ represents the emittance of the cloud. The first two terms are contributions from below the cloud, the third term is the cloud contribution, and the fourth term is the contribution from above the cloud. After some rearranging these expressions can be combined to yield

$$I_\lambda - I_\lambda^{c} = \eta\, (I_\lambda^{cd} - I_\lambda^{c})$$

$$= \eta\, \varepsilon_\lambda \left[B_\lambda(T(p_c))\, \tau_\lambda(p_c) - B_\lambda(T_s)\, \tau_\lambda(p_s) - \int_{p_s}^{p_c} B_\lambda(T(p))\, d\tau_\lambda \right]$$

A simpler form is available by using integration by parts, so

$$I_\lambda - I_\lambda^{c} = \eta\varepsilon_\lambda \int_{p_s}^{p_c} \tau(p)\, \frac{dB_\lambda}{dp}\, dp \, .$$

The techniques for dealing with clouds generally fall into three different categories: (a) searching for cloudless fields of view, (b) specifying cloud top pressure and sounding down to cloud level as in the cloudless case, and (c) employing adjacent fields of view to determine the clear sky signal from partly cloudy observations.

6.2 Inferring Clear Sky Radiances in Cloudy Conditions

Employing adjacent fields of view proceeds as follows. For a given wavelength λ, the radiances from two spatially independent, but geographically close, fields of view are written

$$I_{\lambda,1} = \eta_1 I_{\lambda,1}^{cd} + (1 - \eta_1) I_{\lambda,1}^{c} \quad ,$$

$$I_{\lambda,2} = \eta_2 I_{\lambda,2}^{cd} + (1 - \eta_2) I_{\lambda,2}^{c} \quad ,$$

If the clouds are at a uniform altitude, and the clear air radiance is the same from the two yields of view

$$I_\lambda^{cd} = I_{\lambda,1}^{cd} = I_{\lambda,2}^{cd}$$

and

$$I_\lambda^{c} = I_{\lambda,1}^{c} = I_{\lambda,2}^{c}$$

then

$$\frac{\eta_1 \ (I_\lambda^{cd} - I_\lambda^{c})}{\eta_2 \ (I_\lambda^{cd} - I_\lambda^{c})} = \frac{\eta_1}{\eta_2} = \eta^* = \frac{I_{\lambda,1} - I_\lambda^{c}}{I_{\lambda,2} - I_\lambda^{c}} \ ,$$

where η* is the ratio of the cloud amounts for the two geographically independent fields of view of the sounding radiometer. Therefore, the clear air radiance from an area possessing broken clouds at a uniform altitude is given by

$$I_\lambda^{c} = \frac{I_{\lambda,1} - \eta^* I_{\lambda,2}}{1 - \eta^*}$$

where η* still needs to be determined. Given an independent measurement of the surface temperature, T_s, and measurements $I_{w,1}$ and $I_{w,2}$ in a spectral window channel, then η* can be determined by

$$\eta^* = \frac{I_{w,1} - B_w(T_s)}{I_{w,2} - B_w(T_s)}$$

and I_λ^{c} for the different spectral channels can be solved. Another approach to determining η* is to use simultaneous microwave observations and regression relations between a lower tropospheric microwave sounding brightness temperature and the associated infrared brightness temperatures observed for cloud-free conditions. So if

$$I_{mw} = \sum_\lambda a_\lambda I_\lambda^{c} \quad ,$$

then

$$I_{mw} = \sum_\lambda a_\lambda \frac{I_{\lambda,1} - \eta^* I_{\lambda,2}}{1 - \eta^*} \quad ,$$

and

$$\eta^* = \frac{I_{mw} - \sum_\lambda a_\lambda I_{\lambda,1}}{I_{mw} - \sum_\lambda a_\lambda I_{\lambda,2}} \quad .$$

The partly cloud η* solution has been the basis of the design of the operational infrared sounders

(VTPR, ITPR, HIRS, VAS, and GOES Sounder). The technique is largely credited to Smith. With this correction for cloud contamination, a solution for the temperature profile can be pursued using the techniques presented in this chapter 5.

When there is a differing amount of the same cloud present in two adjacent or nearby fields of view, the cloud corrected radiance is available from the 3.7 and 11.0 micron infrared windows (when reflected sunlight does not interfere with the observations in the shortwave region). Given a partly cloudy atmospheric column then the ratio of the cloud fraction in the two FOVs, η^*, can be estimated from each window channel separately viewing two adjacent fields of view as before

$$\eta^* = \frac{I_{w1,1} - B_{w1}(T_s)}{I_{w1,2} - B_{w1}(T_s)} = \frac{I_{w2,1} - B_{w2}(T_s)}{I_{w2,2} - B_{w2}(T_s)} \quad .$$

T_s is the value that satisfies this equality. Also one can show that

$$B_{w1}(T_s) = A_o + A_1 B_{w2}(T_s)$$

where

$$A_o = \frac{I_{w2,1} I_{w1,2} - I_{w1,1} I_{w2,2}}{I_{w2,1} - I_{w2,2}}$$

and

$$A_1 = \frac{I_{w1,1} - I_{w1,2}}{I_{w2,1} - I_{w2,2}}$$

For constant cloud height and surface temperature conditions, the observed radiances for the two window channels will both vary linearly with cloud amount. As a consequence, cloud amount variations produces a linear variation of the radiance observed in one window channel relative to that radiance observed in another window channel. This linear relation can be used to determine the value of the window radiances for zero cloud amount (N = 0). As shown in Figure 6.1, zero cloud amount must be at the intersection of the observed linear relationship and the known Planck radiance relationship. The brightness temperature associated with this point is the surface temperature. Another common point for the observed and Planck functions is for the case of complete overcast cloud (N = 1). The brightness temperature associated with this point is the cloud temperature. It follows that the constants of the observed linear relationship are the A_o and A_1 constants of the previous equation.

6.3 Finding Clouds

Clouds are generally characterized by higher reflectance and lower temperature than the underlying earth surface. As such, simple visible and infrared window threshold approaches offer considerable skill in cloud detection. However there are many surface conditions when this characterization of clouds is inappropriate, most notably over snow and ice. Additionally, some cloud types such as cirrus, low stratus, and roll cumulus are difficult to detect because of insufficient contrast with the surface radiance. Cloud edges cause further difficulty since the field of view is not always completely cloudy or clear. Multispectral approaches offer several opportunities for improved cloud detection so that many of these concerns can be mitigated. Finally, spatial and temporal consistency tests offer confirmation of cloudy or clear sky conditions.

The purpose of a cloud mask is to indicate whether a given view of the earth surface is unobstructed by clouds. The question of obstruction by aerosols is somewhat more difficult and will be addressed only in passing in this chapter. This chapter describes algorithms for cloud detection and details multispectral applications. Several references are listed as suggested reading regarding cloud detection: Ackerman et al, 1998; Gao et al, 1993; King et al, 1992; Rossow and Garder, 1993; Stowe et al, 1991; Strabala et al, 1994; and Wylie and Menzel, 1999.

In the following sections, the satellite measured visible (VIS) reflectance is denoted as r, and refer to the infrared (IR) radiance as brightness temperature (equivalent blackbody temperature using the Planck function) denoted as Tb. Subscripts refer to the wavelength at which the measurement is made.

6.3.1 Threshold and Difference Tests to Find Clouds

As many as eight single field of view (FOV) cloud mask tests are indicated for daylight conditions (given that the sensor has the appropriate spectral channels). Many of the single FOV tests rely on radiance (temperature) thresholds in the infrared and reflectance thresholds in the visible. These thresholds vary with surface emissivity, atmospheric moisture, aerosol content, and viewing scan angle.

(a) IR Window Temperature Threshold and Difference Tests

Several infrared window threshold and temperature difference techniques are practical. Thresholds will vary with moisture content of the atmosphere as the longwave infrared windows exhibit some water vapour absorption (see Figure 6.2). Threshold cloud detection techniques are most effective at night over water. Over land, the threshold approach is further complicated by the fact that the emissivity in the infrared window varies appreciably with soil and vegetation type (see Figure 6.3). Over open ocean when the brightness temperature in the 11 micron channel (T_{b11}) is less than 270 K, we can safely assume a cloud is present. As a result of the relative spectral uniformity of surface emittance in the IR, spectral tests within various atmospheric windows (such as those at 8.6, 11, and 12 microns respectively) can be used to detect the presence of a cloud. Differences between T_{b11} and T_{b12} have been widely used for cloud screening with AVHRR measurements and this technique is often referred to as the split window technique.

The anticipation is that the threshold techniques will be very sensitive to thin clouds, given the appropriate characterization of surface emissivity and temperature. For example, with a surface at 300 K and a cloud at 220 K, a cloud with emissivity at .01 affects the sensed brightness temperature by .5 K. Since the a noise equivalent temperature of many current infrared window channels is .1 K, the cloud detecting capability is obviously very good.

The basis of the split window technique for cloud detection lies in the differential water vapour absorption that exists between the window channels (8.6 and 11 micron and 11 and 12 micron). These spectral regions are considered to be part of the atmospheric window, where absorption is relatively weak (see Figure 6.2). Most of the absorption lines are a result of water vapour molecules, with a minimum occurring around 11 microns. Since the absorption is weak, T_{b11} can be corrected for moisture absorption by adding the scaled brightness temperature difference of two spectrally close channels with different water vapour absorption coefficients; the scaling coefficient is a function of the differential water vapour absorption between the two channels. This is the basis for sea surface temperature retrievals (see Chapter 6). Thus

$$T_s = T_{b\lambda 1} + a_{PW}\,(T_{b\lambda 1} - T_{b\lambda 2}) \quad ,$$

where a_{PW} is a function of wavelengths of the two window channels and the total precipitable water vapour in the atmosphere.

Thus, given an estimate of the surface temperature, T_s, and the total precipitable water vapour, PW, one can develop appropriate thresholds for cloudy sky detection

$$T_{b11} < 270\ K\ ,$$

$$T_{b11} + a_{PW}\,(T_{b11} - T_{b12}) < T_s\ ,$$

$$T_{b11} + b_{PW}\,(T_{b11} - T_{b8.6}) < T_s\ ,$$

where a_{PW} and b_{PW} are determined from a look up table as a function of total precipitable water vapour. This approach has been used operationally for 6 years using 8.6 and 11 micron bandwidths from the NOAA-10 and NOAA-12 and the 11 and 12 micron bandwidths from the NOAA-11, with a coefficient independent of PW (Menzel *et al* 1993, Wylie *et al* 1994).

The dependence on PW of the brightness temperature difference between the various window channels is seen in Figure 6.4. A global data set of collocated AVHRR 11 and 12 micron and HIRS 8.6 and 11 micron scenes were collected and the total column PW estimated from integrated model mixing ratios to determine a direct regression between PW and the split window thresholds. Linear regression fits indicate the appropriate values for a_{PW} and b_{PW}.

A disadvantage of the split window brightness temperature difference approach is that water vapour absorption across the window is not linearly dependent on PW, thus second order relationships are sometimes used. With the measurements at three wavelengths in the window, 8.6, 11 and 12 micron this becomes less problematic. The three spectral regions mentioned are very useful in determination of a cloud free atmosphere. This is because the index of refraction varies quite markedly over this spectral region for water, ice, and minerals common to many naturally occurring aerosols. As a result, the effect on the brightness temperature of each of the spectral regions is different, depending on the absorbing constituent. Figure 6.5 summarizes the behaviour of the thresholds for different atmospheric conditions.

A tri-spectral combination of observations at 8.6, 11 and 12 micron bands was suggested for detecting cloud and cloud properties by Ackerman *et al*. (1990). Strabala *et al*. (1994) further explored this technique by utilizing very high spatial-resolution data from a 50 channel mutltispectral radiometer called the MODIS Airborne Simulator (MAS). The premise of the technique is that ice and water vapour absorption is larger in the window region beyond 10.5 microns (see Figure 6.6); so that positive 8.6 minus 11 micron brightness temperature differences indicate cloud while negative differences, over oceans, indicate clear regions. The relationship between the two brightness temperature differences and clear sky have also been examined using collocated HIRS and AVHRR GAC global ocean data sets as depicted in Figure 6.7. As the atmospheric moisture increases, $T_{b8.6} - T_{b11}$ decreases while $T_{b11} - T_{b12}$ increases.

The shortwave infrared window channel at 3.9 micron also measures radiances in another window region near 3.5 - 4 microns so that the difference between T_{b11} and $T_{b3.9}$ can also be used to detect the presence of clouds. At night the difference between the brightness temperatures measured in the shortwave (3.9 micron) and in the longwave (11 micron) window regions $T_{b3.9}$-T_{b11} can be used to detect partial cloud or thin cloud within the sensor field of view. Small or negative differences are observed only for the case where an opaque scene (such as thick cloud or the surface) fills the field of view of the sensor. Negative differences occur at night over extended clouds due to the lower cloud emissivity at 3.9 microns.

Moderate to large differences result when a non-uniform scene (e.g., broken cloud) is observed. The different spectral response to a scene of non-uniform temperature is a result of Planck's law; the brightness temperature dependence on the warmer portion of the scene increasing with decreasing wavelength (the shortwave window Planck radiance is proportional to temperature to the thirteenth power, while the longwave dependence is to the fourth power). Table 6.1 gives an example of radiances (brightness temperatures) observed for different cloud fractions in a scene where cold cloud partially obscures warm surface. Differences in the brightness temperatures of the longwave and shortwave channels are small when viewing mostly clear or mostly cloudy scenes; however for intermediate situations the differences become large. It is worth noting in Table 6.1 that the brightness temperature of the shortwave window channel is relatively insensitive to small amounts of cloud (compared to the longwave window channel), thus making it the preferred channel

for surface temperature determinations.

Cloud masking over land surface from thermal infrared bands is more difficult than ocean due to potentially larger variations in surface emittance (see Figure 6.3 and Table 6.2). Nonetheless, simple thresholds can be established over certain land features. For example, over desert regions we can expect that $T_{b11} < 273$ K indicates cloud. Such simple thresholds will vary with ecosystem, season and time of day and are still under investigation.

Brightness temperature difference testing can also be applied over land with careful consideration of variation in spectral emittance. For example, $T_{b11} - T_{b8.6}$ has large negative values over daytime desert and is driven to positive differences in the presence of cirrus. Some land regions have an advantage over the ocean regions because of the larger number of surface observations, which include air temperature, and vertical profiles of moisture and temperature.

Infrared window tests at high latitudes are difficult. Distinguishing clear and cloud regions from satellite IR radiances is a challenging problem due to the cold surface temperatures. Yamanouchi *et al*. (1987) describe a nighttime polar (Antarctic) cloud/surface discrimination algorithm based upon brightness temperature differences between the AVHRR 3.7 and 11 micron channels and between the 11 and 12 micron channels. Their cloud/surface discrimination algorithm was more effective over water surfaces than over inland snow-covered surfaces. A number of problems arose over inland snow-covered surfaces. First, the temperature contrast between the cloud and snow surface became especially small, leading to a small brightness temperature difference between the two infrared channels. Second, the AVHRR channels are not well-calibrated at extremely cold temperatures (< 200 K). Under clear sky conditions, surface radiative temperature inversions often exists. Thus, IR channels whose weighting function peaks down low in the atmosphere, will often have a larger brightness temperature than a window channel. For example $T_{b8.6} > T_{b11}$ in the presence of an inversion. The surface inversion can also be confused with thick cirrus cloud, but this can be mitigated by other tests (e.g., the magnitude of T_{b11} or $T_{b11}-T_{b12}$). Recent analysis of $T_{b11}-T_{b6.7}$ (the 6.7 micron water vapour channel peaks around 400 mb) has shown large negative difference in winter time over the Antarctic Plateau and Greenland, which may be indicative of a strong surface inversion and thus clear skies.

(b) CO_2 Channel Test for High Clouds

A spectral channel sensitive to CO_2 absorption at 13.9 micron provides good sensitivity to the relatively cold regions of the atmosphere. It's weighting function peaks near 300 Hpa, so that only clouds above 500 HPa will have strong contributions to the radiance to space observed at 13.9 microns; negligible contributions come from the earth surface. Thus a 13.9 micron brightness temperature threshold test for cloud versus ambient atmosphere can reveal clouds above 500 HPa or high clouds. This test should be used in conjunction with the near infrared thin cirrus test, described next.

(c) Near Infrared Thin Cirrus Test

This relatively new approach to cirrus detection is suggested by the work of Gao *et al* (1993). A near infrared channel sensitive to H2O absorption at 1.38 micron can be used in reflectance threshold tests to detect the presence of thin cirrus cloud in the upper troposphere under daytime viewing conditions. The strength of this cloud detection channel lies in the strong water vapour absorption in the 1.38 micron region. With sufficient atmospheric water vapour present (estimated to be about 0.4 cm precipitable water) in the beam path, no upwelling reflected radiance from the earth's surface reaches the satellite. The transmittance is given by

$$\tau(p_{sfc}) = \exp(-\delta_{H2O} * \sec\theta_o - \delta_{H2O} * \sec\theta)$$

$$\delta_{H2O} = k_{H2O}\, du$$

As $\tau(p_{sfc}) \rightarrow 0$, $r_{sfc} \rightarrow 0$. τ is the two-way atmospheric transmittance from the top of the atmosphere down to the surface and back to the top of the atmosphere, δ_{H2O} is the water vapour optical depth, θ_o

and θ are the solar and viewing zenith angles respectively, k_{H2O} is the water vapour absorption coefficient, u is the water vapour path length and r_{sfc} is the surface radiance reaching the sensor. Since 0.4 cm is a small atmospheric water content, most of the earth's surface will indeed be obscured in this channel. With relatively little of the atmosphere's moisture located high in the troposphere, high clouds appear bright and unobscured in the channel; reflectance from low and mid level clouds is partially attenuated by water vapour absorption.

Simple low and high reflectance (normalized by incoming solar at the top of the atmosphere) thresholds can be used to separate thin cirrus from clear and thick (near infrared cloud optical depth > ~ 0.2) cloud scenes. These thresholds are set initially using a multiple-scattering model. New injections of volcanic aerosols into the stratosphere impact the thresholds, which thus require periodic adjustment. Any ambiguity of high thin versus low or mid level thick cloud is resolved by a test on the cloud height using a CO_2 sensitive channel at 13.9 microns (see previous section).

(d) Shortwave Infrared Window Reflectance Threshold Test

The reflectance threshold test uses the 3.9 micron channel where values > 6% are considered to be cloudy. However, "cloudy" pixels with 3.9 micron reflectance values < 3% are considered to be snow/ice (Stowe *et al*, 1994). Note that this reflectance test cannot be applied over deserts, as bright desert regions with highly variable emissivities tend to be classified incorrectly as cloudy. Thermal contrast needs to be examined in conjunction with 3.9 micron reflectivity. In addition, thresholds must be adjusted to ecosystem type because of the different surface emissivities (see Table 6.2).

(e) Reflectance Threshold Test

Visible thresholds tests are best used in combination with infrared window observations; during daytime they can be combined as follows. Low reflectance measurements will result from thin cirrus cloud or cloud free conditions, the two being easily separable in the infrared window measurements by the large difference in the emitting temperature of the high cold cirrus and the warm underlying surface. High reflectance measurements result from thick clouds at all levels, and the infrared window brightness temperature provides a good indication of the cloud level. Intermediate reflectance data are subject to ambiguous interpretations since they result from a mixture of cloud and surface contributions.

Visible data used in the determination of the cloud mask must be uncontaminated by sun glint. Algorithms which include solar reflectance data are constrained to solar zenith angles less than 85°. Sun glint occurs when the reflected sun angle, θ_r, lies between 0° and approximately 36°, where

$$\cos\theta_r = \sin\theta \sin\theta_o \cos\phi + \cos\theta \cos\theta_o$$

where θ_o is the solar zenith angle, θ is the viewing zenith angle, and ϕ is the azimuthal angle. Sun glint is also a function of surface wind and sea state.

(f) Reflectance Ratio Test

The reflectance ratio takes advantage of the difference in reflection from cloud versus earth surface in wavelengths above and below 0.75 microns. Many earth surfaces are less reflecting below 0.75 microns than above, but clouds do not exhibit any great difference in reflectance. * Figure 6.8 shows the albedo variations for ice, snow, and vegetation from 0.5 to 3.5 microns. Vegetation shows a sharp increase above 0.72 microns. Snow/ice shows a sharp decrease above 1.4 microns. These step function changes are useful in detecting vegetation or snow/ice versus clouds with spectral band pairs above and below the change. One version of the reflectance ratio test can use the 0.87 micron reflectance divided by 0.66 micron reflectance ($r_{.87}/r_{.66}$). With AVHRR data, this ratio has been found to be between 0.9 and 1.1 in cloudy regions. If the ratio falls within this range, cloud is indicated. New analyses (McClain, 1993) suggest that the minimum value may

need to be lowered to about 0.8, at least for some cases. For cloud-free ocean, the ratio is expected to be less than 0.75 (Saunders and Kriebel, 1988).

(g) Low Cloud Test

Clouds that are low in the atmosphere are often difficult to detect. The thermal contrast between clear sky and low cloud is small and sometimes undetectable by infrared techniques. Reflectance techniques, including the Reflectance Ratio Test (see previous section) can be applied during daylight hours. Use of a channel at .936 microns also offers help under daytime viewing conditions. As documented by the work of Gao and Goetz (1991), this channel is strongly affected by low level moisture. When low clouds are present they obstruct the low level moisture, hence increasing the reflectance. A reflectance ratio of .936 over .865 microns, an atmospheric window with similar surface reflectance characteristics also shows promise.

(h) Microwave Tests

The brightness temperature of a lower tropospheric sounding microwave channel can be regressed against the brightness temperatures of several lower tropospheric infrared sounding channels for clear situations. Therefore the microwave brightness temperature for a given fov can be calculated from the observed infrared brightness temperatures. This will be valid in clear sky conditions only. If the observed microwave brightness temperature is greater than the calculated, it is indicative of cloud contamination in the infrared observations and the fov should be classified accordingly.

(i) Resultant Cloud Mask

All of the single pixel tests mentioned so far rely on thresholds. Thresholds are never global. There are always exceptions and the thresholds must be interpreted carefully. For example, the reflectance ratio test identifies cloud for values in the range 0.9 to 1.1. However, it seems unrealistic to label a pixel with the ratio = 1.1 as cloudy, and a neighbouring pixel with the ratio of 1.11 as non-cloudy. Rather, as one approaches the threshold limits, the certainty or confidence in the labelling becomes more and more uncertain. An individual confidence flag must be assigned and used with the single pixel test results to work towards a final determination.

Each threshold determination is pass, conditional pass, or fail along with a confidence assessment. Conditional pass involves those radiances that fall within an uncertainty region of the threshold. The uncertainty is a measure of instrument noise in that channel and the magnitude of the correction due to non blackbody surface emissivity as well as atmospheric moisture and/or aerosol reflection contributions. The individual confidence flag indicates a one, two, or three sigma confidence level for each single pixel test result. The initial FOV obstruction determination is a sum of the squares of all the confidence flags and single pixel test results.

6.3.2 Spatial Uniformity Tests To Find Cloud

When the single field of view tests do not definitively determine an unobstructed FOV, spatial and temporal consistency tests are often useful. Temporal consistency compares composited previous 30 day clear sky radiances and yesterday's cloud mask to today's clear sky single pixel results. Spatial consistency checks neighbouring clear sky pixel radiances (same ecosystem). If any consistency test fails, the confidence in the final cloud/no cloud determination is reduced by 1 sigma level.

(a) Infrared Window One-Dimensional Histogram Tests

One-dimensional histogram tests have a long history of determining clear sky scenes. As with the IR threshold tests, it is most effective over water and must be used with caution in other situations. The method is physically based on the assumption that for a uniform scene, such as a small geographic region of the ocean, the observed radiances will be normally distributed, the width of the normal curve defined by the instrument noise. This test is not a single FOV test, but requires

a number of observations over a given region with similar surface radiative properties. To improve the clear sky estimate, the histogram can be constructed only from the FOVs that pass one or more of the single FOV thresholds previously discussed. A one-dimensional IR channel histogram is constructed over a given geographical region (with 1km FOVs an area of 10 km x 10 km is appropriate). A gaussian function is fit to the warmest peak of the histogram; the temperature (T_{peak}) and the noise limits (σ) are determined. The clear sky brightness temperature threshold is the temperature that corresponds to one-sigma (σ) towards the cold side of the gaussian function peak.

$$T_{thres} = T_{peak} - \sigma \ .$$

An example of this approach is demonstrated in Figure 6.9 using AVHRR global observations.

(b) Infrared Window Radiance Spatial Uniformity

The infrared window spatial uniformity test (often applied on 10 by 10 pixel segments) is also most effective over water and must be used with caution in other situations. Most ocean regions are well suited for spatial uniformity tests; such tests may be applied with less confidence in coastal regions or regions with large temperature gradients (e.g. the Gulf Stream). The spatial coherence test is based on the assumption of a uniform background and singled-layered, optically thick cloud systems. The emitted radiance is

$$I = (1 - A_c)\, I_{clr} + A_c\, I_{cld}$$

The method is based upon the computation of the mean and standard deviation for a group of pixels using 11 micron radiances. When the standard deviation is plotted versus the mean an arch shaped structure is often observed (see Figure 6.10). The feet with low standard deviations are associated with clear sky for high mean values and cloudy conditions for low mean values. The clear sky FOVs can be selected as those within a standard deviation threshold (which is fixed at a small value) of the warm foot of the arch. Note that the derived clear sky foot of the arch should have a temperature consistent with the thresholds derived using the individual FOV tests. Uniform stratus can also give the appearance of a uniform ocean, thus the spatial tests must often complement the threshold tests (e.g., the tri-spectral test).

Surface temperature variability, both spatial and temporal, is larger over land than ocean, making land scene spatial uniformity tests difficult. If the spatial uniformity tests over land are constrained to similar ecosystems, then better results are obtained.

The spatial coherence method developed by Coakley and Bretherton (1982) is recognized for being especially useful in determining clear and cloudy sky radiances over uniform backgrounds. It has been applied to single-layered and sometimes multi-layered cloud systems that extend over moderately large regions, greater than $(250\ km)^2$, and which have completely cloudy and completely clear pixels. The spatial coherence test is not run over regions of varying topography; however, it is applied for relatively homogeneous topographical regions of similar ecosystem.

(c) Visible Reflectance Uniformity Test

A reflectance uniformity test can be applied by computing the maximum and minimum values of the .66 micron channel and the 0.87 micron channel reflectances within a 10 x 10 pixel array. Pixel arrays with 0.66 micron reflectance differences greater than threshold 1 (around 9%) over land or 0.87 micron reflectance differences greater than threshold 2 (possibly 0.3%) over ocean are labelled as mixed (Stowe *et al*., 1993). The value over ocean is low because a cloud-free ocean is almost uniformly reflective, while non-uniformity is assumed to be caused by cloudiness. This test again works better by requiring that the ecosystem be the same for the pixel array. Further, the reflectance threshold is a function of satellite zenith and view angle.

(d) Two-Dimensional Infrared and Visible Histogram Analysis

As with the 1-D histogram approach, 2-D histograms can be used which make use of the

measurements of IR emitted radiances as well as the reflected solar visible radiances. A 2-D Gaussian surface can be fitted to the peak with the warmest temperature and/or lowest reflectance. The Gaussian surface equation is

$$G(IR,VIS) = G_{peak} \exp[- P(IR,VIS)]$$

with

$$P(IR,VIS) = (Tb-Tb_{peak})^2 /\sigma_{IR}^2 - 2(Tb-Tb_{peak})(r-r_{peak})/\sigma_{IR}\sigma_{VIS} + (r-r_{peak})^2/\sigma_{VIS}^2$$

where σ_{IR} and σ_{VIS} are the IR and VIS standard deviation respectively; VIS and IR are measurements in the solar and IR. VIS channels may be replaced with NIR channels when necessary. The solar and infrared radiances can be a combination of various channels. The best solar channels to use are those for which the difference in reflectance between cloud and water is a maximum.

6.4 The Cloud Mask Algorithm

The tests detailed in the previous sections are applied as follows. Single pixel threshold tests are engaged first. If the confidence level reads uncertain (less than 2 sigma confidence), then spatial uniformity tests on 10 by 10 pixel segments are used. Temporal and spatial continuity tests follow; these utilize data from 50 by 50 pixel segments, the cloud mask from yesterday, and the clear sky radiance composite from the last month.

6.4.1 Thick High Clouds (Group 1 Tests)

Thick high clouds are detected with threshold tests that rely on brightness temperatures in three infrared spectral bands; they are BT_{11}, $BT_{13.9}$, and $BT_{6.7}$. Infrared window thresholds, BT_{11}, are practical in certain conditions, however they will vary with moisture content of the atmosphere. Over land, BT_{11} is further complicated by the fact that the surface emissivity varies appreciably with soil and vegetation type. Thus, BT_{11} is used primarily to detect high, thick clouds and thresholds are set accordingly. For example, clouds are likely present when BT_{11} is less than 270 K over tropical oceans. $BT_{13.9}$ provides good sensitivity to the relatively cold regions of the atmosphere because of CO_2 absorption. The same is true for $BT_{6.7}$ because of H_2O absorption. These spectral bands receive most of their radiation near 300 hPa and only clouds above 500 hPa make strong radiance contributions; negligible contributions come from the earth surface. Thus a threshold for $BT_{13.9}$ and $BT_{6.7}$ can isolate clouds above 500 hPa.

6.4.2 Thin Clouds (Group 2 Tests)

Thin clouds tests rely on brightness temperature difference tests BT_{11}- BT_{12}, $BT_{8.6}$ - BT_{11}, BT_{11}- $BT_{3.9}$, and, BT_{11}- $BT_{6.7}$. These tests will catch many of the clouds missed by the thick high cloud tests. Differences between BT_{11} and BT_{12} have been widely used for cloud screening with AVHRR measurements; this technique is often referred to as the split window technique.

Split window techniques have been used operationally for more than 6 years using 8.6 and 11 μm bandwidths from the NOAA-10 and NOAA-12 and the 11 and 12 μm bandwidths from the NOAA-11, with a coefficient independent of precipitable water [Menzel *et al*. 1993, Wylie *et al*. 1994]. The tri-spectral combination of observations at 8.6, 11 and 12 μm bands [Ackerman *et al*. 1990, Strabala *et al*. 1994] is being tested. $BT_{8.6}$ - BT_{11} greater than zero indicates cloud, while negative differences, over oceans, indicate clear regions. As atmospheric moisture increases, $BT_{8.6}$ - BT_{11} decreases while BT_{11} - BT_{12} increases.

Brightness temperature difference techniques for many of the infrared window spectral bands on the newer sensors with better than .05 K noise are being used successfully in thin clouds.

At night positive values of $BT_{3.9}$- BT_{11} are used to detect partial cloud or thin cloud within the

sensor field of view. Negative differences occur over extended clouds due to the lower cloud emissivity at 3.9 μm. In daylight hours, solar reflection at 3.9 μm is used for detecting water clouds.

In polar regions during winter, large negative values in $BT_{8.6}$ - BT_{11} during winter time over the Antarctic Plateau and Greenland indicate a strong surface inversion and thus clear skies. This test is proving useful in the MODIS cloud mask algorithm.

6.4.3 Low Clouds (Group 3 Tests)

Low clouds are best detected using solar reflectance tests that include reflectance thresholds ($r_{0.87}$, $r_{0.65}$, and $r_{.936}$), reflectance ratio tests, and brightness temperature differences $BT_{3.9}$-$BT_{3.7}$. These tests work well when there is a high contrast in the reflectance between the surface and the cloud, for example, clouds over dark vegetation and water. Group 3 tests complement Group 1 tests; Group 3 is sensitive to thick, low level clouds while Group 1 has difficulty with low clouds that have small thermal contrast between cloud and background. Spectral reflectance thresholds are routinely used in many cloud detection algorithms. A wide variety of thresholds exist in the literature, depending on surface type and solar and view angle geometry. It is likely that pre-launch threshold estimates will require adjustment post-launch.

The reflectance ratio ($r_{0.87}/r_{0.66}$) is between 0.9 and 1.1 in cloudy regions and outside in clear regions. The lower value is adjusted to below 0.75 for cloud-free ocean.

The shortwave infrared window bands at 3.7 and 3.9 μm are also used to detect the presence of clouds. Over land, longwave infrared window spectral variation in surface emissivity presents difficulties for brightness temperature difference tests. Shortwave infrared window spectral variation in surface emissivity is much smaller for some ecosystems, while spectral variation in cloud emissivity remains substantial. Thus brightness temperature differences between $BT_{3.7}$ and $BT_{3.9}$ are usually small in clear sky but larger in clouds. During the daylight hours the difference increases because of the increased solar energy at 3.7 μm.

6.4.4 High Thin Clouds (Group 4 Tests)

Initial detection of high thin clouds is attempted with a threshold test at 1.38 μm. No upwelling reflected radiance from the earth's surface reaches the sensor when sufficient atmospheric water vapor is present (estimated to be about 0.4 cm precipitable water) in the FOV. Simple low and high reflectance thresholds are used to separate thin cirrus from clear and thick (near-infrared cloud optical depth > ~ 0.2) cloud scenes.

Further detection of high thin cirrus is attempted with inspection of brightness temperature difference tests BT_{11}- BT_{12}, BT_{12}- BT_4, and $BT_{13.7}$- $BT_{13.9}$. The Group 4 tests are similar to those in Group 2, but they are specially tuned to detect the presence of thin cirrus. BT_{11}- BT_{12} is greater than zero in ice clouds due to the larger absorption at the longer wavelength in the infrared window. BT_{12}-BT_4 is less than zero in semitransparent cirrus as subpixel warm features dominate the shortwave window radiances within a FOV. $BT_{13.7}$- $BT_{13.9}$ is nominally positive in clear skies, but goes to zero when viewing cirrus. The large differences between ground and cloud temperatures make these tests useful for thin cirrus detection.

6.4.5 Ancillary Data Requirements

A number of preprocessing steps are necessary before a cloud masking algorithm is applied. First, each pixel in the scene must be tagged as being land or water, and if land, a land/water percentage. Second, each land pixel must be designated as relatively flat, valley, isolated mountainous region, low mountains or hills, generally mountainous, or extremely rugged mountains. Each pixel must also be designated as probably/probably not snow covered. Each land pixel must be classified as to its ecosystem, along with a more general ecosystem classification of urban, forest, woodland, grassland, shrub land, tundra, arid vegetation and highland vegetation. Ocean regions must be classified as water, coastline (including islands), possibility of isolated icebergs, marginal ice zone, and nearly solid sea ice (leads may be present). This requires ancillary

data described below.

Earth surface character type must be available in various databases which categorize features such as:

- salt or lake bed
- flat or relatively flat desert (or for high latitudes, glaciers or permanent ice)
- marsh
- lake country or atoll
- major valleys or river beds
- isolated mountains, ridge or peak
- low mountains
- mountainous
- extremely rugged mountains
- ocean

The different surface emissivities should be estimated according to different ecosystems. Table 6.5 shows some representative values for the infrared windows. Also Figure 6.3 provides further information.

Sea ice coverage is available from the US NAVY/NOAA Sea Ice Product, which provides weekly reports of fractional ice coverage at spatial resolution of about 18 km.

Snow cover is available in the NOAA Snow Data Product, which provides weekly reports of snow cover at a spatial resolution of 150-200 km; snow is reported if the grid cell is more than 50% covered.

Information on surface temperature and sea state is available from surface observations, Reynolds blended analysis, and NMC model 3-hour surface analyses of temperature and wind speed.

6.4.6 Implementation of the Cloud Mask Algorithms

The cloud mask has the following stages:

(a) Note pixels that have sun glint (possible effect on visible tests);

(b) Note pixels that have high solar zenith angle (possible effect on visible tests);

(c) Apply single FOV masking tests and set initial unobstructed FOV determination:
IR temperature threshold and difference tests;
CO_2 test for high clouds;
Near infrared thin cirrus test;
SWIR Reflectance threshold test;
Reflectance ratio test;
Low cloud test;
microwave test.

(d) Check for consistency:
clear FOVs in same ecosystem have similar radiances;
compare with clear sky composites from yesterday and from the past month (if clear today is radiance within sigma interval of past clear).

(e) If pixel is uncertain, use spatial uniformity tests in 10 x 10 pixel regions:
Spatial IR uniformity test applied using $\sigma = 3.5$ K;
Spatial reflectance uniformity test;
IR and VIS 2-D histogram test.

(f) Reset quality flag if successful in increasing confidence levels.

6.4.7 Short-term and Long-term Clear Sky Radiance Composite Maps

Composite maps have been found to be very useful. A cloud mask must rely on composite maps, but good spatial resolution and the many spectral bands mitigate the dependence. Clear-sky reflectance and temperature composites have been successfully used to detect clouds by comparing the pixel radiances to the clear-sky composite values with some added thresholds (Rossow and Garder 1993). These composites are based on the observation that variations in VIS clear reflectances usually are smaller in time than in space, especially over land. Variations of surface VIS reflectances generally are smaller than variations of cloud reflectances. Therefore, it is assumed that the characteristic shape of the darker part of the VIS radiance distribution is at most weakly dependent upon surface type (Seze and Rossow, 1991a, b). The minimum reflectance values are used to estimate clear values. Corrections to the minimum values are inferred from the shapes of the visible reflectance distribution associated with different surface types.

Rossow and Garder (1993) classify the surface into nine types depending on the time scale and magnitude of the reflectance variations (see below). The clear sky reflectance values for land and ocean regions whose surface characteristics vary the most rapidly are estimated. Sparsely vegetated surfaces generally exhibit more spatial variability than heavily vegetated surfaces (cf. Matthews and Rossow, 1987), but are also generally less cloudy. Sparsely vegetated arid regions generally exhibit more spatial variability (Matthews and Rossow, 1987) and are less cloudy. Vegetated areas show less small scale spatial variability. They also tend to be more uniform from one geographic location to another. Individual pixel reflectance values within each latitude zone are compared to the distributions of values for the same ecosystem type; they are required to be within some limit of the distribution mode value. Similar assumptions are used for the determination of clear sky temperature fields.

6.5 Cloud Properties Derived in a MODIS Granule

MODIS cloud products are generated on a granule basis; a granule is 5 minutes of data and consists of approximately 2100 along-track pixels. The suite of operational cloud products begins with cloud detection or masking (i.e., deciding whether or not a cloud is present). Infrared techniques are employed to estimate cloud top pressure, effective cloud amount (product of cloud fraction and cloud emittance), and cloud thermodynamic phase. In daytime data, cloud optical thickness and effective particle size is provided using solar reflectance techniques. A cirrus reflectance retrieval is provided separately. The following sections provide background on the methodology used to infer these various parameters. With the exception of the cloud mask, all cloud products are archived in a single Hierarchical Data Format (HDF) file with the product designation MOD06; the cloud mask product is in product MOD35.

6.5.1 Cloud Masking

The MODIS cloud mask product serves as the primary ancillary input to the other cloud algorithms (Ackerman et al., 1998). The focus of the product is to indicate a level of confidence as to whether the pixel is unobstructed between the surface and satellite. In addition to the potential for obstruction in the line of sight due to clouds, heavy aerosols (e.g., smoke) and dust will also act to decrease the likelihood of finding clear-sky conditions. The product provides more information than a simple yes/no decision; there are 48 bits of output per 1-km pixel that includes information on sets of multispectral test results, the processing path, and limited ancillary information such as a land/ocean tag. The first eight bits provide a summary sufficient for most applications. Additionally, the first two bits simply offer information in four categories: *confident clear, probably clear, uncertain*/*probably cloudy*, and *cloudy*.

The algorithm uses a variety of multispectral tests (see previous sections) involving combinations of up to 19 spectral bands. The use of these bands change somewhat as calibration issues are mitigated. Different sets of tests are applied depending on the surface (land, water,

snow/ice, desert, and coast) and solar illumination (day/twilight/night). In addition to the multispectral tests, a textural test is applied over ocean to improve the detection of dust.

Several ancillary data sets are used in the cloud clearing process. Surface snow and ice data are provided by the Near Real-Time Ice and Snow Extent (NISE) product from the National snow and Ice Data Center, and the NOAA National Center for Environmental Prediction (NCEP) 0.5^{o} resolution sea concentration product. The NCEP Reynolds blended SST product (Reynolds and Smith, 1994) has been implemented to improve the product at nighttime over oceans and in areas where there are strong temperature gradients such as in the vicinity of the Gulf Stream.

6.5.2 Cloud Thermodynamic Phase

There are currently three inferences of cloud phase found in the MOD06 cloud product: a bispectral IR algorithm, a set of shortwave IR (SWIR) tests, and a decision tree algorithm that includes cloud mask results as well as the IR and SWIR tests. The latter two phase retrievals are stored in the MODIS "Quality_Assurance_1km" output. The decision tree algorithm gives the phase that was used in the subsequent optical and microphysical retrieval. The current IR phase algorithm is at a 5 km spatial resolution, while the other two are at 1 km. This section will summarize the IR phase retrieval (Baum et al., 2000). Details on the SWIR and decision tree phase tests can be found in Platnick et al. (2003).

The IR phase retrieval provides four categories: *ice, water, mixed phase*, and *uncertain*. A "mixed phase" cloud is thought to consist of a mixture of ice and water particles. With the IR-based method, cloud phase is inferred from the brightness temperature difference (BTD) between the 8.5 and 11 μm brightness temperatures (BTD[8.5-11]) as well as the 11μm brightness temperature. The physical basis for this approach stems from the observation that the imaginary component of the index of refraction (m_i) differs for ice and water at these two wavelengths. The BTD[8.5-11] is affected by atmospheric water vapor absorption, surface emissivity, and cloud particle size (small particles scatter more radiation than large particles). Radiative transfer simulations show that for ice clouds, the BTD[8.5-11] values tend to be positive in sign, whereas for low-level water clouds, the BTD[8.5-11] values tend to be very negative. This simple bi-spectral IR technique is adequate for classifying the phase as either "ice" or "water" for about 80% of the cloudy pixels on a global basis. The most problematic areas are optically thin cirrus, multilayered clouds (especially thin cirrus over lower-level water clouds), and single-layered clouds having cloud top temperatures between 233K and 273K (i.e., supercooled water or "mixed phase" clouds). Supercooled water or mixed-phase clouds tend to occur most frequently in the high latitude storm belts of both hemispheres.

To improve the inference of cloud phase during daytime, the IR tests are supplemented by reflectances obtained at a visible (e.g., 0.65 μm) wavelength and a near-infrared (NIR) wavelength (e.g., 1.64 μm or 2.15 μm). At wavelengths less than about 0.7 μm, clouds composed of either liquid or ice tend to absorb very little solar radiation. However, at the NIR wavelength, the imaginary index of refraction values for both water and ice increase in comparison with those at the visible wavelength, but also diverge from each other with values for ice being greater than for water. Even with these supplementary tests, mixed-phase clouds remain a challenge.

Figure 6.11 shows a false color image from MODIS taken 1 July 2003 at 1458 UTC that contains a high-level ice cloud deck that overlies a low-level water deck in numerous places. High ice clouds are distinguished from low water-phase clouds in the IR cloud phase estimations.

6.5.3 Cloud Top Pressure and Effective Cloud Amount

For the past several decades, a technique known as CO_2 slicing has been used to infer cloud-top pressure and effective cloud amount (the product of the cloud fraction and the cloud emittance) from radiances measured in spectral bands located within the broad 15-μm CO_2 absorption region. The term *effective cloud amount* is sometimes referred to as *effective emissivity* in the literature. As the wavelength increases from 13.3 μm to 15 μm, the atmosphere becomes more opaque due to CO_2 absorption, thereby causing radiances obtained from these spectral bands to be sensitive to a different portion of the atmosphere. This technique has been applied to data

from the High resolution Infrared Radiometer Sounder (HIRS; Wylie and Menzel 1999) as well as the Geostationary Operational Environmental Satellite (GOES) sounder (Menzel et al. 1992; Menzel and Purdom 1994). The field of view (FOV) size for HIRS at nadir is approximately 18 km and for GOES is 10 km. MODIS provides measurements at 1-km resolution and at four wavelengths located in the broad 15-μm CO_2 band, but cloud top properties are produced at 5-km spatial resolution. It is hoped that future products will provide all cloud top property results at the full 1-km resolution.

The MODIS cloud pressure is converted to cloud height and cloud temperature through the use of gridded meteorological products that provide temperature profiles at some nominal vertical resolution every 6 hours. The product used for this purpose is the NCEP Global Data Assimilation system (GDAS). (Derber et al. 1991). Model calculated radiances should be made to match measured radiances to avoid modest height assignment errors. There are many benefits to the CO_2 slicing algorithm, foremost of which is its unique heritage and application to data spanning a record of more than 25 years. Cloud properties are derived similarly for both daytime and nighttime data as the IR method is independent of solar illumination. This approach is very useful for the analysis of midlevel to high-level clouds, and especially semi-transparent clouds such as cirrus. One constraint to the use of the 15 μm channels is that the cloud signal (change in radiance caused by the presence of cloud) becomes comparable to instrument noise for optically thin clouds and for clouds occurring in the lowest 3 km of the atmosphere. When low clouds are present, the 11 μm data are used to infer cloud top temperature and then pressure and height via model analysis.

Figure 6.12 shows an example cloud top pressure product from MODIS.

6.5.4. Cloud Optical and Microphysical Properties

Cloud optical thickness is defined as the vertical integration of extinction over the cloud physical thickness. For water clouds composed of spherical particles, effective particle size is defined as the ratio of the third moment to the second moment of the particle size distribution. The definition of effective particle size for ice clouds is made more difficult because ice particles tend to be nonspherical. For ice clouds, the definition of particle size is proportional to the ratio of the total volume to the projected area of the ice particles for a given size and habit distribution.

The simultaneous retrieval of optical thickness and effective particle size derived from cloud reflectance measurements in solar band atmospheric windows is well known. MODIS retrievals are performed using a band that is practically non-absorbing for bulk water/ice (0.65, 0.86, or 1.2 μm) combined with three longer wavelength bands where bulk water/ice has significant absorption (1.6, 2.1, and 3.7 μm). Three separate effective sizes are provided in MOD06 corresponding to each of these absorbing bands. The 3.7 μm band includes a significant thermal emission component in addition to the solar reflectance component. The 2.1 μm size retrieval is considered the default value for Level-3 aggregations (discussed in next section). MODIS is the first imager to take measurements in each of these bands simultaneously. The retrievals are based on library calculations of plane parallel homogeneous clouds overlying a black surface in the absence of an atmosphere. Separate libraries have been built for water and ice clouds; currently no separate library exists for mixed phase clouds.

Surface albedo effects and corrections for atmospheric transmittance are accounted for on a pixel basis during operational processing. Since cloud reflectance over land is significantly affected by the underlying surface albedo, significant effort has been made to improve this aspect of the retrievals. Toward this end, the MODIS operational surface spectral albedo/BRDF (bidirectional reflectance distribution function) product (MOD43) provides 16-day composites of clear-sky observations at 1-km spatial resolution for both BRDF and albedo. The spectral albedo product includes solar illumination and diffuse sky values. These properties are provided for all the relevant MODIS solar bands (except at 3.7 μm). From these 16-day composites, a full year of data has been composited and aggregated by land cover type to determine the extent to which ecosystem can be used as a predictor to spectral albedo. The MODIS land cover product (MOD12) is also used in this effort. A sinusoidal fit between the summer/winter extremes is made to replicate the seasonal cycle. For operational processing, snow and ice cover is provided by the NISE product; when snow or ice is present, spectral albedos are provided from field measurements. Further details regarding the

MODIS retrieval algorithm are described in Platnick et al. (2003).

6.5.5 Detection of Multilayered Clouds

Satellite-based cloud property retrievals are performed under the assumption that any individual set of radiance measurements for a given field of view contains a single cloud layer. The retrieved cloud top properties will contain the least error if the uppermost cloud layer is optically thick (i.e., opaque). However, observation indicates that multilayered clouds are common, especially for the case in which semi-transparent ice cloud overlies lower-level water clouds. In this situation, the assumption of a single cloud layer results in a cloud top pressure that lies between that of the upper and lower cloud layers. Error in the cloud top pressure propagates into errors in the inferred optical and microphysical properties.

New research is being conducted to determine when cirrus overlies water clouds in daytime conditions. While many approaches are being tested, the approach described here is based on NIR-IR bands at 1.6/2.1 and 11 μm, respectively. As noted previously in the discussion on cloud phase, ice particles absorb more radiation than water particles at the NIR wavelengths (1.6/2.1 μm). Ice clouds also tend to reside at much higher altitudes than water clouds. The specific assumptions invoked for each pixel array (nominally 200 *x* 200 pixels) are that at most two distinct cloud layers are present, any pixels not uniquely associated with either of the two distinct cloud layers are classified as being multilayered, clouds of both ice and water phase are present, knowledge of the clear-sky NIR/IR properties must be known, and a separation distance of at least 2 km in height exists between the layers.

The MOD35 cloud mask product provides information regarding clear and cloudy pixels, and cloud thermodynamic phase is assessed using the 8.5 μm and 11 μm brightness temperatures. Although either the 1.6- or 2.1-μm reflectance bands can be used in the multilayered cloud detection technique, the 2.1-μm band is used for the Aqua data because a number of the 1.6-μm band detectors on the Aqua MODIS instrument are inoperative (the band is comprised of 20 total detectors). To provide a confidence level to the assessment of whether a pixel contains more than one cloud layer, the method is applied as the pixel array, or tile, is moved gradually across the data granule, thereby testing each pixel (away from the granule borders) multiple times. The more times a pixel is flagged as containing multiple cloud layers, the higher the confidence in that assessment.

6.5.6. Global Gridded (Level-3) Products

Once the Level-2 granule-level cloud products have been produced, spatial and temporal composites are aggregated to daily, eight-day, and monthly data. Statistics are sorted onto a $1^o \times 1^o$ equal-angle grid containing *180 x 360* individual cells. The Level-3 atmosphere product, MOD08, is derived separately for Aqua and Terra. For the daily product, every Level-2 granule that overlaps any part of the data day, defined as being from 0000 to 2400 UTC, is included in the compositing process. A granule that spans either 0000 UTC or 2400 UTC may be included in two consecutive MOD08 daily products. The eight-day product is derived from the daily Level-3 products summarized over eight consecutive days. The eight-day intervals are reset at the beginning of each year similarly to the Level-3 products produced by the MODIS ocean and land discipline groups. The monthly product provides a summary of the daily products obtained over a calendar month.

While there is no separation of the cloud parameters by ascending or descending node, there is a day/night separation and a process/no process decision for a number of parameters. Cloud fraction (from the cloud mask) and cloud top properties (i.e., cloud pressure and IR phase) are processed for both day and night and are provided in the Level-3 products as daytime only, nighttime only, and combined day and night. Cloud optical and microphysical properties are summarized for daytime only since they are not derived at night. The cloud fraction derived from the cloud mask is currently provided by name “Cloud_Fraction_IR”. A daytime-only cloud fraction is also derived from successful optical and microphysical retrievals and aggregated by thermodynamic phase as well as all phases. As an example, the name for the liquid phase cloud fraction is “Cloud_Fraction_Water” (Platnick et al., 2003).

The Level-3 products also include histograms of cloud parameters and joint histograms derived from comparison of two parameters. Approximately 13 joint histograms are derived from the MOD06 cloud product. Ten of these are aggregated by cloud phase (5 for liquid water clouds and 5 for ice clouds). The joint histograms are computed from the following list: cloud optical thickness, effective particle size, cloud-top temperature, and effective cloud amount. The other three joint histograms are aggregated by solar illumination (day, night, or combined day and night) and are built from cloud-top pressure and effective cloud amount.

Futher Level-3 algorithm and aggregation details, along with example images, can be found in King et al. (2003).

6.6 Ongoing Cloud Climatologies

Several cloud studies have been ongoing for some time. The following paragraphs summarize a few.

The International Satellite Cloud Climatology Project (ISCCP) has developed cloud detection schemes using visible and infrared window radiances. The NOAA Cloud Advanced Very High Resolution Radiometer (CLAVR) algorithm uses the five visible and infrared channels of the AVHRR for cloud detection using spectral and spatial variability tests. CO_2 Slicing characterizes global high cloud cover, including thin cirrus, using infrared radiances in the carbon dioxide sensitive portion of the spectrum. Additionally, spatial coherence of infrared radiances in cloudy and clear skies has been used successfully in regional cloud studies. The following paragraphs briefly summarize these prior approaches.

6.6.1 ISCCP

The ISCCP algorithm is described by Rossow (1989, 1993), Rossow *et al*. (1989), Seze and Rossow (1991) and Rossow and Garder (1993). Only two channels are used, the narrow band visible (0.6 micron) and the infrared window (11 micron). Each observed radiance value is compared against its corresponding Clear-Sky Composite value. Clouds are assumed to be detected only when they alter the radiances by more than the uncertainty in the clear values. In this way the "threshold" for cloud detection is the magnitude of the uncertainty in the clear radiance estimates.

The ISCCP algorithm is based on the premise that the observed VIS and IR radiances are caused by only two types of conditions, 'cloudy' and 'clear', and that the ranges of radiances and their variability that are associated with these two conditions do not overlap (Rossow and Garder 1993). As a result, the algorithm is based upon thresholds, where a pixel is classified as "cloudy" only if at least one radiance value is distinct from the inferred "clear" value by an amount larger than the uncertainty in that "clear" value. The uncertainty can be caused both by measurement errors and by natural variability. This algorithm is constructed to be "cloud-conservative," minimizing false cloud detections but missing clouds that resemble clear conditions.

The ISCCP cloud-detection algorithm consists of five steps (Rossow and Garder 1993): (1) space contrast test on a single IR image; (2) time contrast test on three consecutive IR images at constant diurnal phase; (3) cumulation of space/time statistics for IR and VIS images; (4) construction of clear-sky composites for IR and VIS every 5 days at each diurnal phase and location; and (5) radiance threshold for IR and VIS for each pixel. ISCCP detects high clouds from (a) only infrared 11 μm window channel data where it misses some thin cirrus clouds because there is no correction for the transmission of terrestrial radiation through the clouds; and (b) infrared window data corrected for cloud semi-transparency using the solar reflection measurements at 0.6 μm with a radiative transfer model. ISCCP D2 data can be obtained from the Web page at http://isccp.giss.nasa.gov/dataview.html.

6.6.2 CLAVR

The NOAA Cloud and AVHRR algorithm uses all five channels of AVHRR (0.63, 0.86, 3.7,

11.0, 12.0 micron) to derive a global cloud mask (Stowe *et al*., 1991). It examines multispectral information, channel differences, and spatial differences and then employs a series of sequential decision tree tests. Cloud free, mixed (variable cloudy) and cloudy regions are identified for 2x2 global area coverage (GAC) pixel (4 km resolution) arrays. If all four pixels in the array fail all the cloud tests, then the array is labelled as cloud-free (0% cloudy); if all four pixels satisfy just one of the cloud tests, then the array is labelled as 100% cloudy. If 1 to 3 pixels satisfy a cloud test, then the array is labelled as mixed and assigned an arbitrary value of 50% cloudy. If all four pixels of a mixed or cloudy array satisfy a clear-restoral test (required for snow/ice, ocean specula reflection, and bright desert surfaces) then the pixel array is re-classified as "restored-clear" (0% cloudy). The set of cloud tests is subdivided into daytime ocean scenes, daytime land scenes, nighttime ocean scenes and nighttime land scenes.

Subsequent improvements to the CLAVR, now under development, will use dynamic clear/cloud thresholds predicted from the angular pattern observed from the clear sky radiance statistics of the previous 9-day repeat cycle of the NOAA satellite for a mapped one degree equal area grid cell (Stowe *et al*., 1994). As a further modification, CLAVR will include pixel by pixel classification based upon different threshold tests to separate clear from cloud contaminated pixels, and to separate cloud contaminated pixels into partial and total (overcast) cover. Cloud contaminated pixels will be radiatively "typed" as belonging to low stratus, thin cirrus, and deep convective cloud systems. A fourth type indicates all other clouds, including mixed level clouds.

6.6.3 CO_2 slicing

CO_2 slicing (Wylie *et al*., 1994) has been used to distinguish transmissive clouds from opaque clouds and clear sky using High resolution Infrared Radiation Sounder (HIRS) multispectral observations. With radiances around the broad CO_2 absorption band at 15 microns, clouds at various levels of the atmosphere can be detected. Radiances from near the centre of the absorption band are sensitive to only upper levels while radiances from the wings of the band (away from the band centre) see successively lower levels of the atmosphere. The CO_2 slicing algorithm determines both cloud level and cloud amount from radiative transfer principles. It has been shown to be especially effective for detecting thin cirrus clouds that are often missed by simple infrared window and visible approaches. Difficulties arise when the spectral cloud forcing (clear minus cloudy radiance for a spectral band) is less than the instrument noise. The technique is described in more detail in Chapter 8.

A statistical summary of over 76 million cloud observations from HIRS since 1979 is shown in Table 6.3. In Table 6.3a, high clouds above 440 hPa comprise 33% of the observations. 18% of the observations are of clouds between 440 hPa and 700 hPa. Low clouds below 700 hPa are found 24% of the time. Cloud free conditions are found 25% of the time. Cirrus and transmissive clouds (with effective emissivities less than 0.95) are found in 43% of our observations; they range from 100 to 800 hPa. The 13% transmissive observations below 440 hPa are most likely broken clouds. Clouds opaque to infrared radiation (with effective emissivities greater than 0.95) are found 32% of the time. Table 6.3b shows the same cloud statistics corrected for the fact that HIRS does not observe lower cloud layers where higher cloud layers are found. This random overlap assumption yields more representative of lower cloud coverages. Cloud frequency statistics are reported both ways in the literature, with and without correction for high cloud blockage. Accounting for blockage by high clouds, low clouds are inferred to be observed in 49% of the observations. The global average cloud effective emissivity (global average of $N\varepsilon$) is found to be 0.54; Warren *et al*. (1988) report a global cloud fraction of 0.61 from ground observations.

Figure 6.13 shows the geographical distribution of all clouds in the summer and winter seasons. The months of December, January, and February represent the boreal winter (austral summer) and the months of June, July, and August represent the boreal summer (austral winter). The seasonal summaries are compiled using a uniformly spaced grid of 2^o latitude by 3^o longitude. Each grid box for each season has at least 1000 observations. The Inter-Tropical Convergence Zone (ITCZ) is readily discernible as the region of more frequent clouds; the mid-latitude storm belts are also evident. The ITCZ is seen to move north with the sun from boreal winter to summer. The subtropical high pressure systems are seen in the regions of less frequent cloud cover. Over the

Indonesian region the ITCZ expands in latitudinal coverage from boreal winter to summer. In the central Pacific Ocean, the ITCZ shows both a southern and northern extension during the boreal winter months. In the southern hemisphere, the eastern Pacific Ocean off South America and the eastern Atlantic Ocean off Africa remain relatively free of clouds throughout the year. The southern hemispheric storm belt is evident throughout the year. In the northern hemisphere's mid-latitude storm belts, the frequency of clouds increases during the winter with the strengthening of the Aleutian Low in the north Pacific Ocean and the Icelandic Low in the north Atlantic Ocean. The North American cloud cover shows little seasonal change. Large convective development occurs during the austral summer (boreal winter) in South America and Africa, which is readily apparent in the increased detection of clouds. Some regions exhibit cloudy conditions for a complete season. In two grid boxes in the African ITCZ (8N, 10.5W and 2N, 19.5E), all HIRS observations found cloud during all boreal summers of this study. Eight grid boxes were cloudy for all boreal winters of this study; four were located in the central Amazon (centered at 8S, 58W), two in the African Congo (6S, 26E), and two in the Indonesian area (2S, 113E and 4S, 146E). With each grid box covering approximately 75,000 square kilometers, in the boreal winter there are about 300,000 square kilometers in the Amazon that are always cloud covered. There were no grid boxes where all HIRS observations found cloud in all seasons.

Observations of clouds above 6 km (Figure 6.13) exhibit the same general geographical patterns found for total clouds. They are most predominant in the tropical ITCZ and move with the seasons. During the boreal winter in a few areas such as Southern Brazil, Tropical South Africa and Indonesia, high clouds are found in more than 90% of the observations. Less frequent occurrence is found in the mid-latitude storm belts. Differences in observations of high clouds and observations of all clouds are evident in the subtropical highs over the extra-tropical oceans where marine stratus clouds are prevalent and higher clouds are far less frequent. This is evident along the west coasts of North and South America and Africa.

Figure 6.14 shows the frequency of cirrus detection in the HIRS cloud studies since 1979. Globally averaged frequency of cloud detection (excluding the poles where cloud detection is less certain) has stayed relatively constant at 75%; there are seasonal fluctuations but no general trends. High clouds in the upper troposphere (above 6 km) are show a small increasing trend of ~ 2% per decade.

The geographical locations of the cloud cover changes are studied using the difference of the average of the 1990s of the HIRS record subtracted from the average of 1980s (see Figure 6.15). Overall, the decadal average cloud cover has not changed appreciably from the 1980s to the 1990s. Small increases occurred in the tropics, mainly in the Indonesian Islands. Small decreases occurred in the sub-tropics, the eastern Sahara and in the central Pacific Ocean from Hawaii westward. The decreasing trend in Antarctica is uncertain because cloud detection itself is very difficult in the cold temperatures of Antarctica. Increases of 10% in the last decade for clouds above 6 km altitude occurred in the western Pacific, Indonesia, and over Northern Australia. Other fairly large increases occurred in western North America, Europe, the Caribbean, Western South America, and the Southern Ocean north of Antarctica. Decreases in high clouds occurred mainly in the tropical South Pacific, Atlantic and Indian Oceans south of the ITCZ.

While jet aircraft have been suspected of increasing cirrus cloud cover from their contrails, these data do not reveal such a trend. Increases of high clouds seem to occur in areas of high air traffic, such as central and western North America and Europe, as well as areas of rare air traffic, such as the Southern Ocean around Antarctica. It appears that high cloud cover changes are mostly caused by larger weather systems. The most significant feature of these data may be that the globally averaged cloud cover has shown little change in spite of dramatic volcanic and El Nino events. Figure 6.16 shows that during the four El Nino events winter clouds moved from the western Pacific to the Central Pacific Ocean, but their global average in the tropics did not change. El Chichon and Pinitubo spewed volcanic ash into the stratosphere that took 1-2 years to fall out, but cloud cover was not affected significantly.

These cloud data show overall constancy, with a small increase in high clouds. The high thin clouds capture some of the earth's infrared radiation similar to CO2 and thus they contribute to

global warming in the same manner. Clouds do not appear to be off-setting global warming by increasing their reflection of incoming solar radiation; they are possibly enhancing it with modest increase of thermally trapping high thin ice clouds.

References

Ackerman S. A., K. I. Strabala, W. P Menzel, R. E. Frey, C. C. Moeller, and L. E. Gumley, 1998: Discriminating clear sky from clouds with MODIS, *J. Geophys. Res.,* **103**, pp. 32141-32157.

Baum B. A., D. P. Kratz, P. Yang, S. Ou, Y. X. Hu, P. F. Soulen, and S. C. Tsay, 2000: Remote sensing of cloud properties using MODIS Airborne Simulator imagery during SUCCESS. I. Data and models, *J. Geophys. Res*., 105, pp. 11,767-11,780

Derber, J. C., D. F. Parrish, and S. J. Lord,1991: The new global operational analysis system at the National Meteorological Center, *Weather Forecasting*. **6**, pp. 538-547

King, M. D., W. P. Menzel, Y. J. Kaufman, D. Tanré, B. C. Gao, S. Platnick, S. A. Ackerman, L. A. Remer, R. Pincus, and P. A. Hubanks, 2003: Cloud, Aerosol and Water Vapor Properties from MODIS., *IEEE Trans. Geosci. Remote Sens.*, **41**, pp. 442-458

Menzel W. P., D. P. Wylie, and K. I. Strabala, 1992: Seasonal and diurnal changes in cirrus clouds as seen in four years of observations with the VAS, *J. Appl. Meteor*., **31**, 370-385

Menzel W. P. and J. F. W. Purdom, 1994: Introducing GOES-I: The first of a new generation of Geostationary Operational environmental Satellites. *Bull. Amer. Meteor. Soc.,* Vol. **75**, No. 5, pp. 757-781

Moeller, C. C., H. E. Revercomb, S. A. Ackerman, W. P. Menzel, and R. O. Knuteson, 2003: Evaluation of MODIS thermal IR band L1B radiances during SAFARI 2000. *J. Geophys. Res.*, **108**, D13, 8494.

Platnick S, M. D. King, S. A. Ackerman, W. P. Menzel, B. A. Baum, J. C. Riédi, R. A. Frey, 2003: The MODIS cloud products: algorithms and examples from Terra. *IEEE Trans. Geosci. Remote Sens.*, **41**, pp. 459-473

Reynolds W. R., T. M. Smith, 1994: Improved global sea surface temperature analyses using optimum interpolation. *J. Climate*, **7**, 929-948

Strabala K. I., S.A. Ackerman, and W. P. Menzel, 1994: Cloud properties inferred from 8-12 μm data, *J. Appl. Meteorol.*, **2,** pp. 212-229

Wylie D. P. and W. P Menzel, 1999: Eight years of global high cloud statistics using HIRS. *J. Clim.,* **12**, 170-184

Wylie, D. P., D. L. Jackson, W. P. Menzel, and J. J. Bates, 2005: Global Cloud Cover Trends Inferred from Two decades of HIRS Observations. Accepted by Jour Clim.

Table 6.1 Longwave and Shortwave Window Planck Radiances (mW/m**2/ster/cm-1) and Brightness Temperatures (degrees K) as a function of Fractional Cloud Amount (for cloud of 220 K and surface of 300 K) using $B(T) = (1-N)*B(T_{sfc}) + N*B(T_{cld})$.

Cloud Fraction N	Longwave Window Rad	Temp	Shortwave Window Rad	Temp	$T_s - T_1$
1.0	23.5	220	.005	220	0
.8	42.0	244	.114	267	23
.6	60.5	261	.223	280	19
.4	79.0	276	.332	289	13
.2	97.5	289	.441	295	6
.0	116.0	300	.550	300	0

Table 6.2 Estimates of emissivities for different surface types

	(3.5-3.9)	(10.3-11.3)	(11.5-12.5)
Rocks:			
Igneous			
Granite.h2	.91	.91	.95
Andesite.h1	.96	.90	.95
Basalt.h1	.96	.90	.95
Sedimentary			
Limestone.h1	.89	.94	.97
Sandstone.h1	.83	.96	.98
Shale.h1	.86	.97	.98
Metamorphic			
Marble.h2	.94	.95	.98
Quartzite.h1	.78	.97	.98
Schist.h3a	.90	.94	.96
Slate.h1a	.89	.95	.97
Soils:			
Entisols			
(quartz-rich)	.85	.97	.98
Vertisols			
(high clay content)	.87	.97	.98
Aridisols			
(desert,fine quartz, clay, carbonate soil)	.75	.97	.97
Mollisols			
(black organic-rich)	.83	.97	.98
Vegetation			
Lichens	.95	.97	.98
Green Foliage			
Beech	.95	.95	.96
Hickory	.95	.98	.98
Red Oak	.97	.95	.95
Conifer	.98	.98	.98
Indian Grass	.97	.96	.98
Senescent Foliage			
Sen Beech	.75	.82	.85
Sen Red Oak	.84	.91	.92
Sen Pine	.96	.98	.98
Sen Rye Grass	.85	.91	.91
Decomposing Soil Litter			
Deciduous	.92	.96	.96
Coniferous	.94	.98	.98
Seawater and Distilled	.97	.99	.99
Ice			
Sea Ice smooth	.96	.98	.97
Sea Ice 100 grit	.93	.99	.97
Water Coatings			
Foam	.97	.99	.99
Oil 42667	.96	.96	.96
Soil Float	.97	.98	.98

(Estimates made from average reflectance values reported in Salisbury and D'Aria (1992, 1994)).

Table 6.3a UW NOAA Pathfinder HIRS cloud reports by cloud height and density from 1979-2001. $N\varepsilon$ refers to effective emissivity, and σ refers to the corresponding visible optical depth. Over 76,000,000 HIRS observations from 9 NOAA satellites are included. Percentages of all observations are reported.

	Cloud Density			
	Thin	Thick	Opaque	
Cloud Level	$N\varepsilon < 0.5$ $\sigma_{vis} < 1.4$	$0.5 < N\varepsilon < 0.95$ $1.4 < \sigma_{vis} < 6$	$N\varepsilon > 0.95$ $\sigma_{vis} > 6$	***All Densities***
High (<440 hPa)	15 %	15 %	3 %	33 %
Middle (440-700 hPa)	5 %	7 %	6 %	18 %
Low (>700 hPa)		1 %	23 %	24 %
Total	20 %	23 %	32 %	75 %

Table 6.3b:Table 6.3a statistics which have been corrected for the number of times the middle and low layers were actually observed by HIRS using the random overlap assumption.

	Cloud Density			
	Thin	Thick	Opaque	
Cloud Level	$N\varepsilon < 0.5$ $\sigma_{vis} < 1.4$	$0.5 < N\varepsilon < 0.95$ $1.4 < \sigma_{vis} < 6$	$N\varepsilon > 0.95$ $\sigma_{vis} > 6$	***All Densities***
High (<440 hPa)	15 %	15 %	3 %	33 %
Middle (440-700 hPa)	7 %	10 %	9 %	26 %
Low (>700 hPa)		2 %	47 %	49 %
Total	20 %	23 %	32 %	75 %

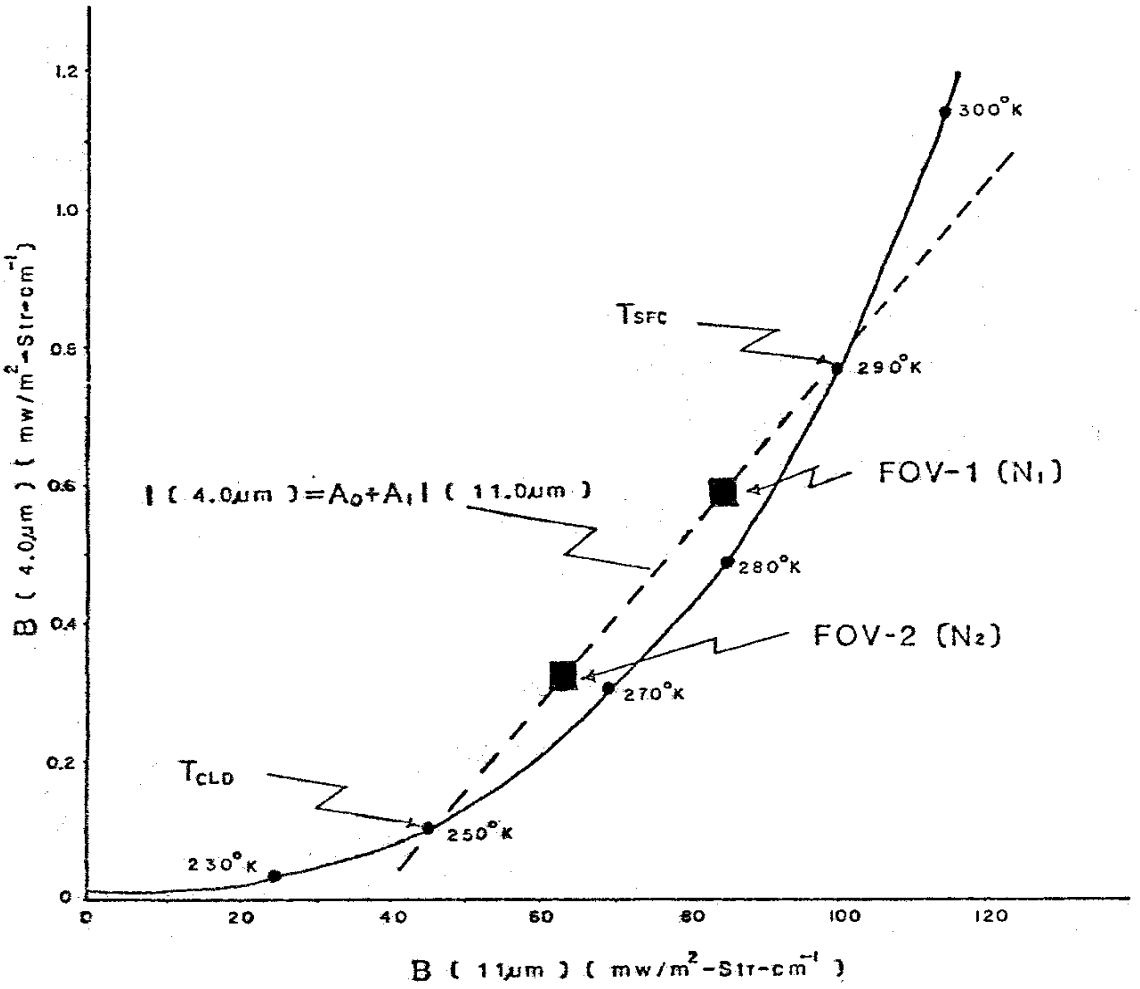

Figure 6.1: Ratio of the radiances for the two window channels; solid curve is the theoretical cloud free curve and dashed curve is the linear variation with cloud amount.

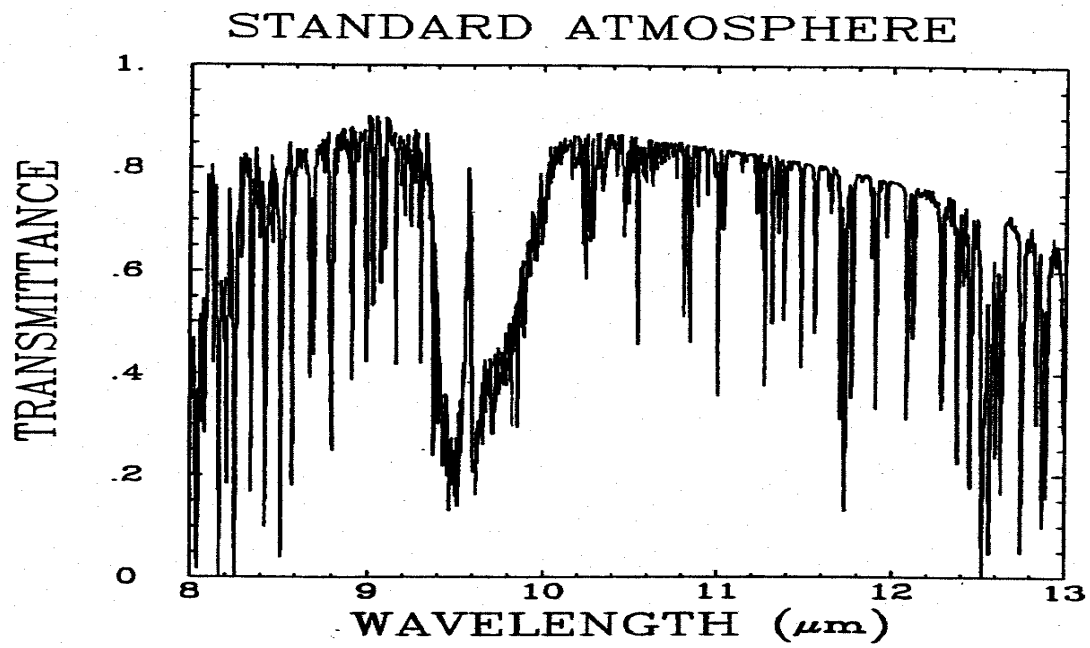

Figure 6.2. High spectral resolution total transmittance spectra for a standard atmosphere from 8 to 13 micron.

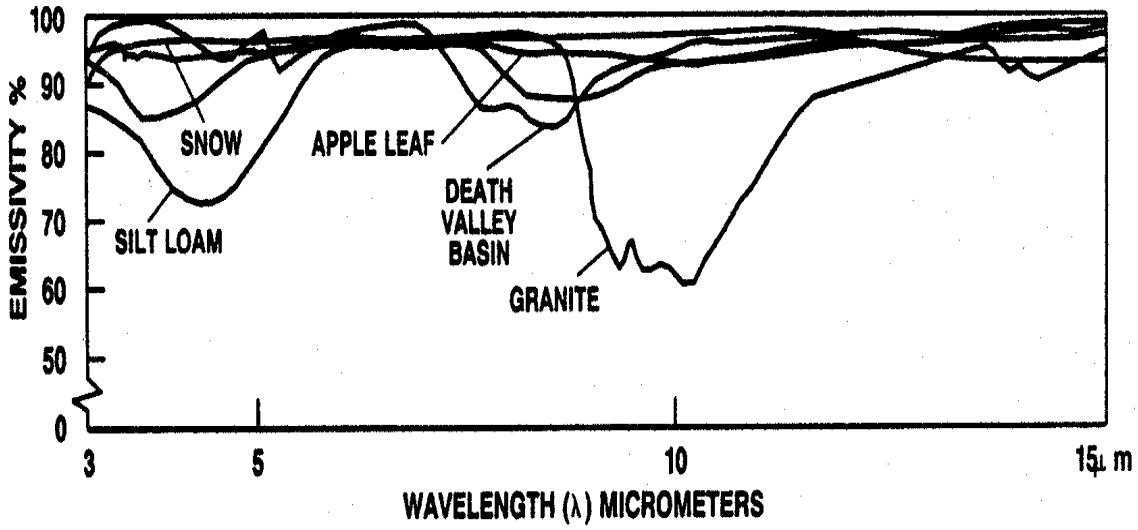

Figure 6.3. Emissivity of various soil and vegetation types as a function of wavelength.

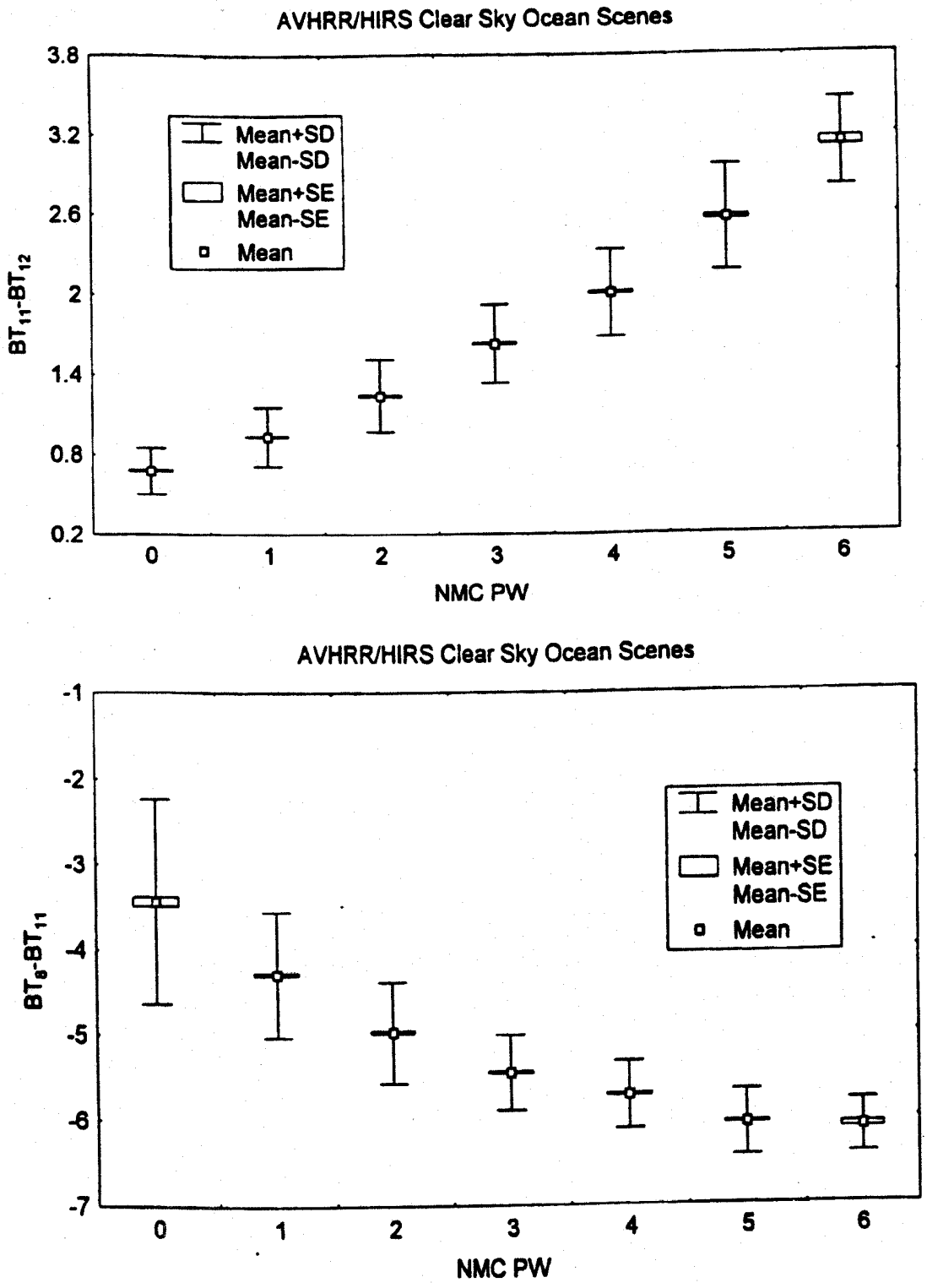

Figure 6.4. The dependence on PW of the brightness temperature difference between the various window channels. Observed AVHRR 11-12 micron (top panel) and collocated HIRS 8-11 micron (bottom panel) brightness temperature differences plotted versus global model (NMC) total column PW for January 1994 over clear ocean scenes.

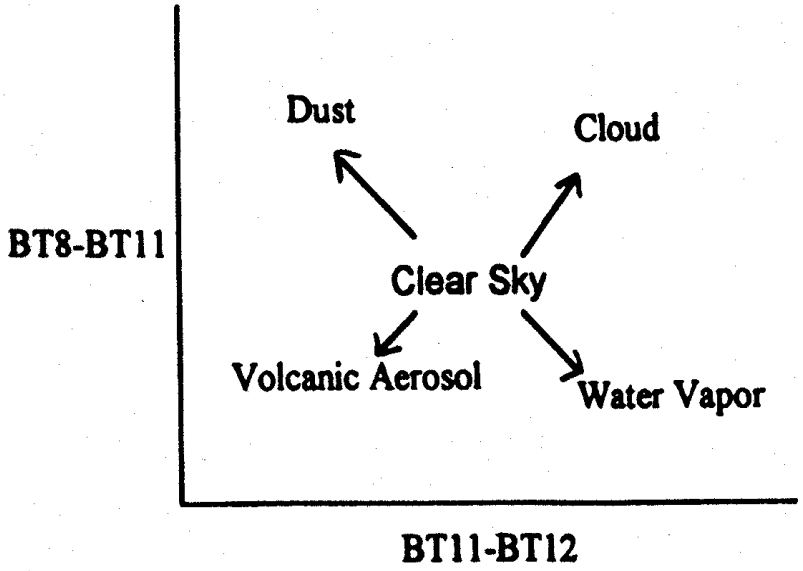

Figure 6.5. Schematic diagram of the effects of different atmospheric constituents on the brightness temperature differences 11 minus 12 microns and 8.6 minus 11 microns.

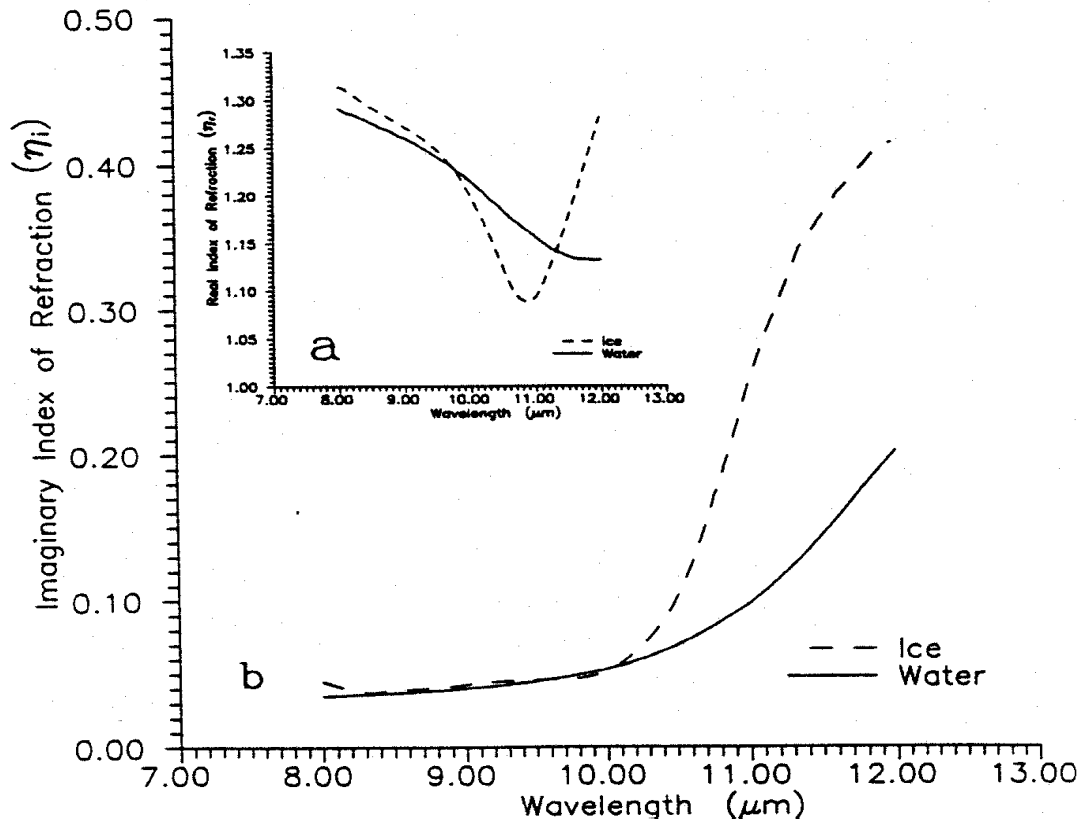

Figure 6.6. Indices of refraction of ice and water across the window region (a) real part and (b) imaginary part (associated with absorption). Note the greater absorption of ice over water for wavelengths greater than 10.5 microns.

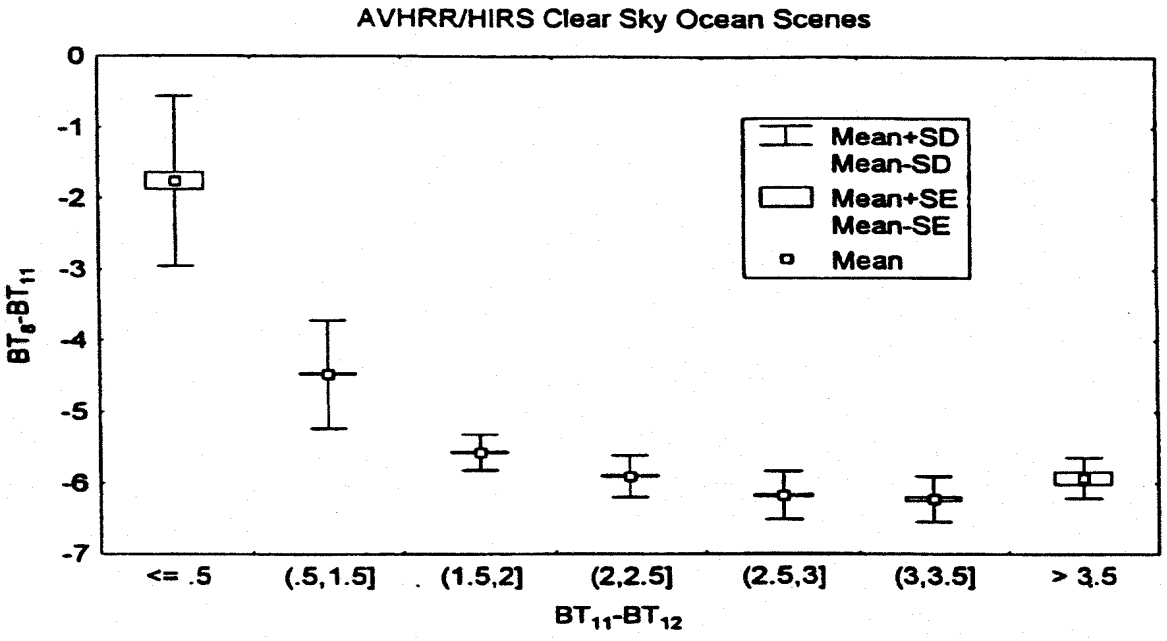

Figure 6.7. Scatter diagram of collocated HIRS 8-11 versus AVHRR 11-12 micron brightness temperature differences for January 1994 over clear ocean scenes. As moisture increases, the 11-12 micron brightness temperature difference increases while the 8888-11 micron brightness temperature difference decreases.

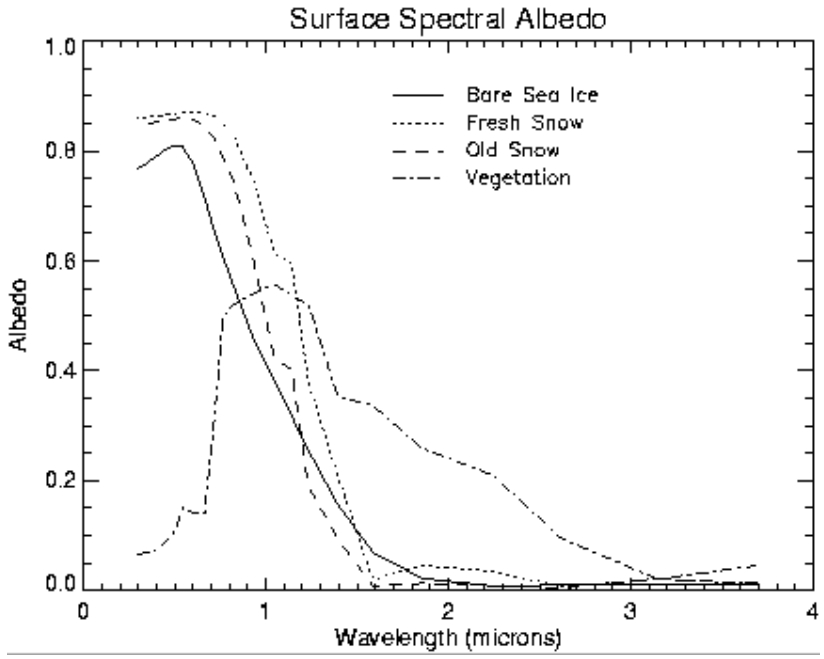

Figure 6.8. Albedo variations for ice, snow, and vegetation from 0.5 to 3.5 microns. Vegetation shows a sharp increase above 0.72 microns. Snow/ice shows a sharp decrease above 1.4 microns.

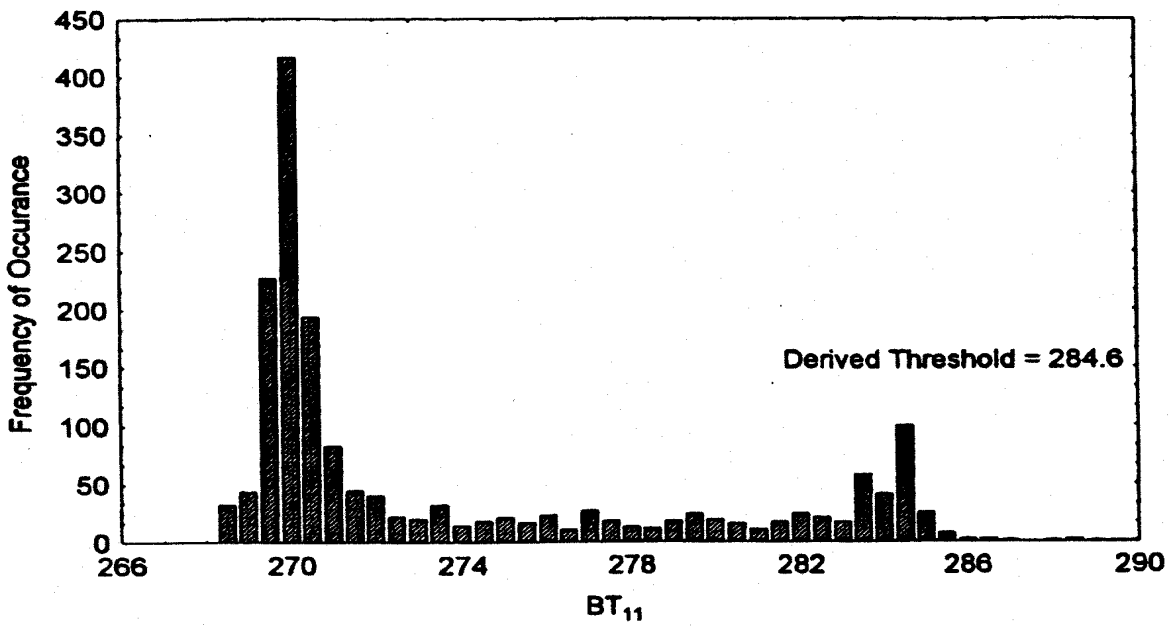

Figure 6.9. Example of infrared histogram analysis technique using AVHRR data for 2.5 by 2.5 degree ocean region. The derived clear sky brightness temperature threshold is 284.6 K.

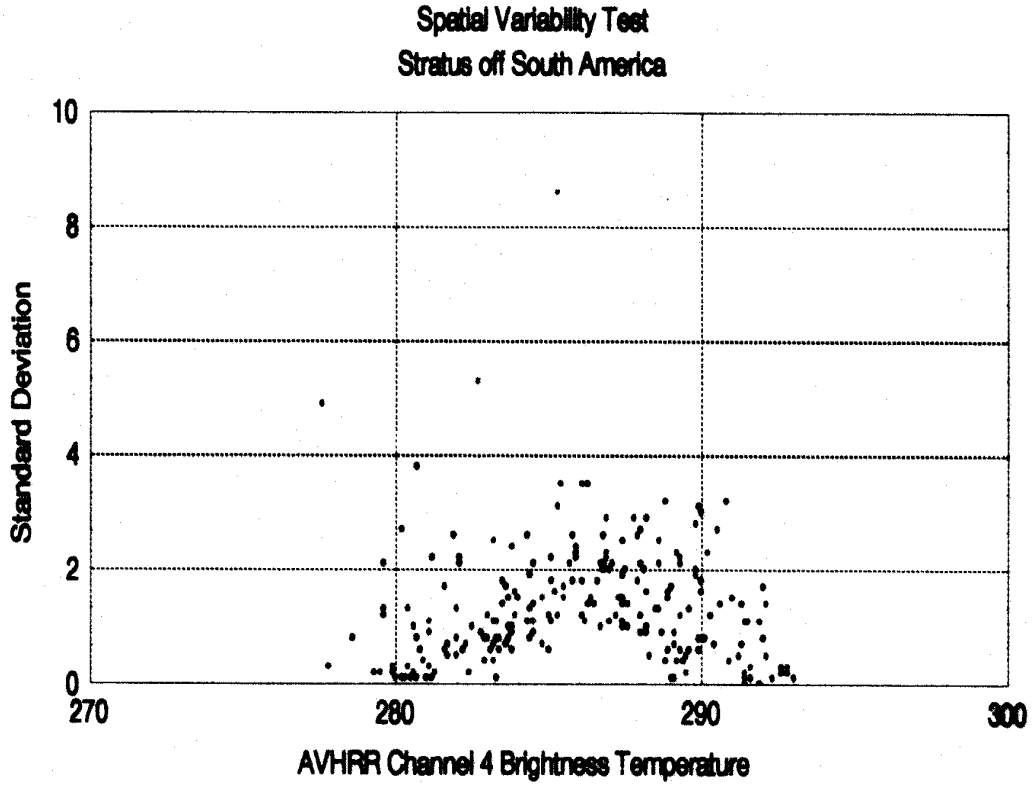

Figure 6.10. Example of the arches obtained when plotting local deviation from mean with respect to temperature.

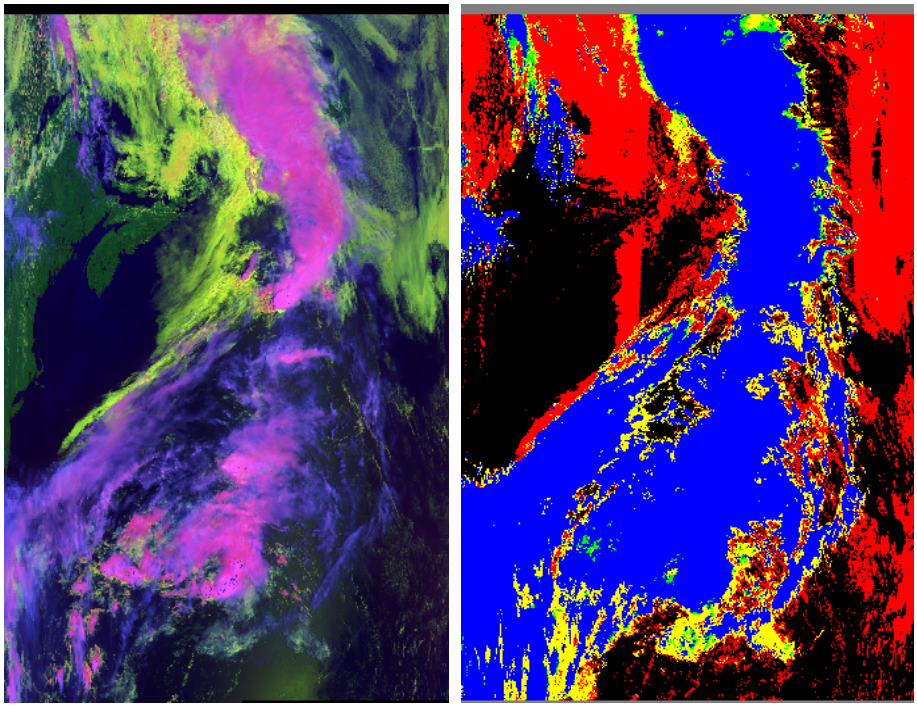

Figure 6.11: (Left) False color image (R: band 1, G: band 6, and B: band 31, flipped). High ice clouds are pink or blue, low water-phase clouds are yellow, land is green, and water is dark blue. (Right) IR cloud phase with ice clouds (blue), water clouds (red), mixed phase clouds (green), and uncertain phase (yellow).

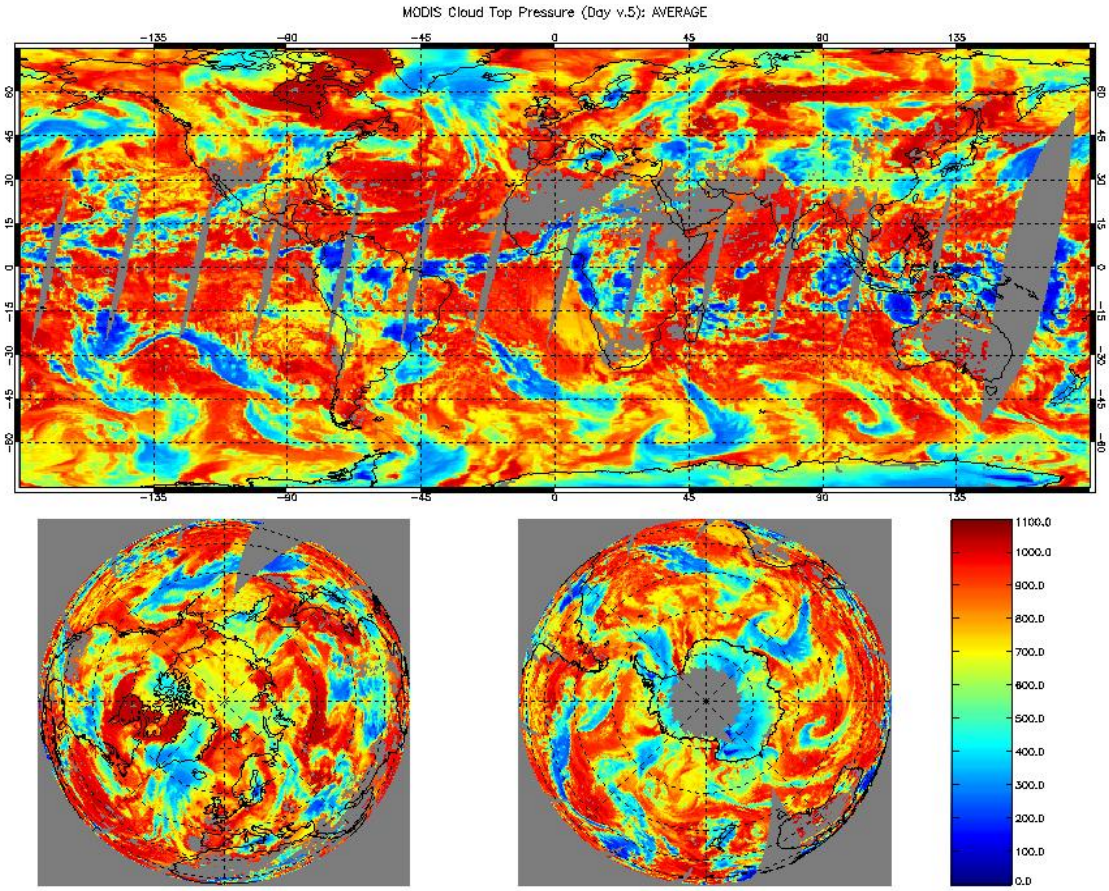

Figure 6.12: MODIS Cloud Top Pressures inferred from the CO2 slicing technique for 4 April 2003. Mid-latitude cloud bands are clearly evident.

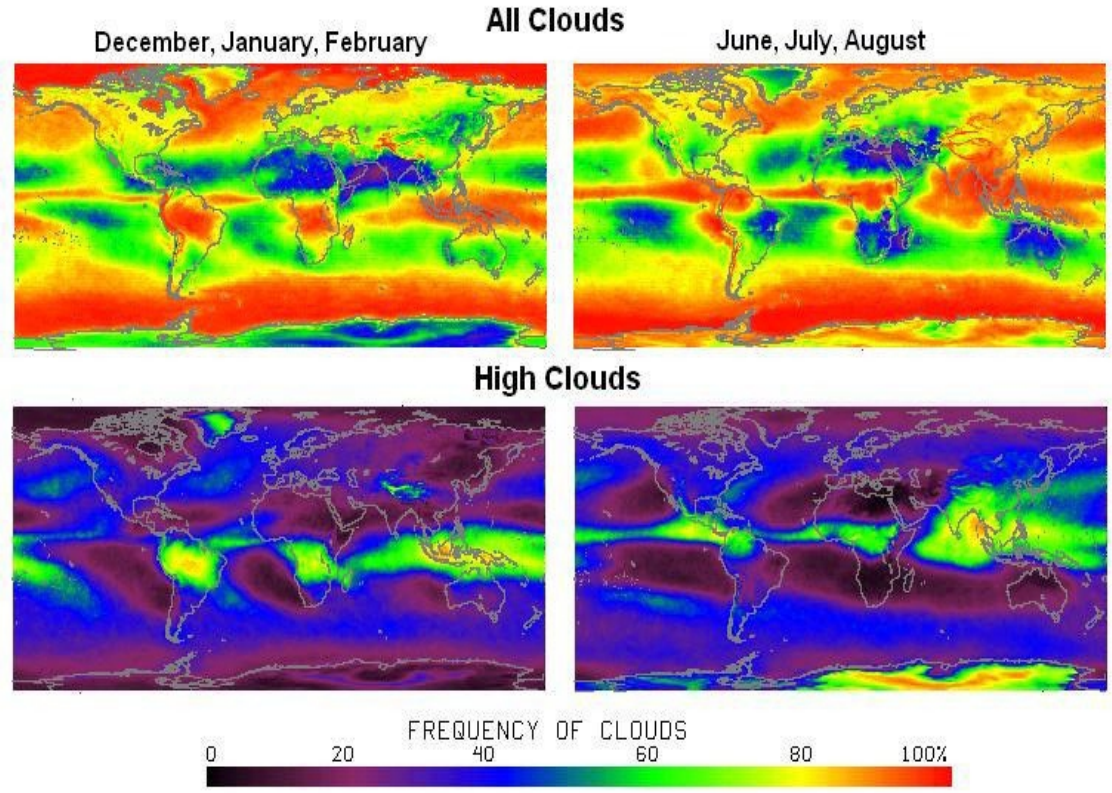

Figure 6.13: The frequency of all clouds and high clouds above 440 hPa from 1979 to 2001 found in HIRS data during winter (December, January, February) and summer (June, July, August).

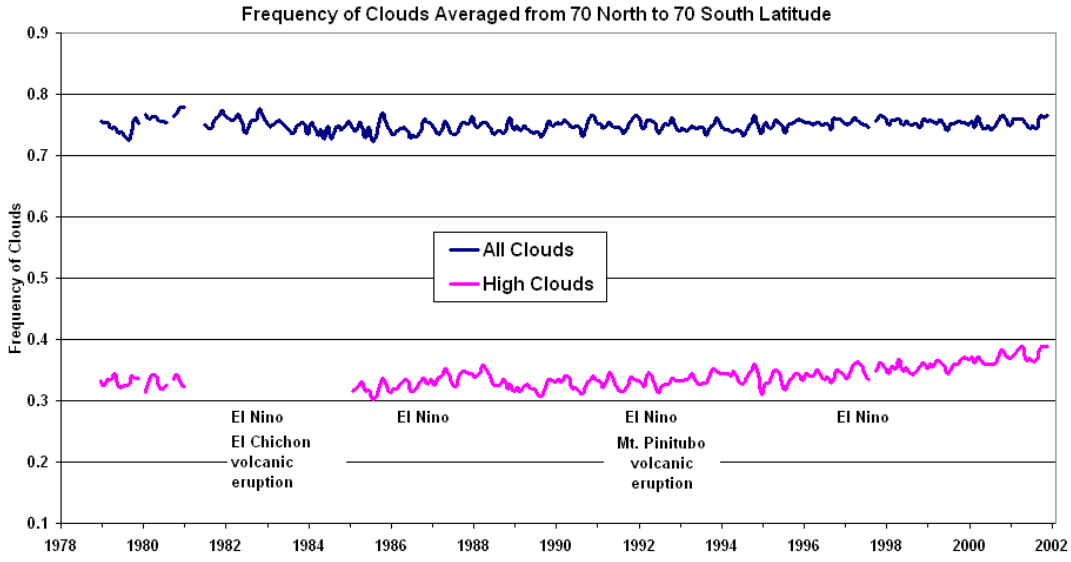

Figure 6.14: The global frequency of all and high (above 6 km) cloud detection in a HIRS FOV since 1979 (excluding the poles where cloud detection is less certain). Major climatic events are also indicated.

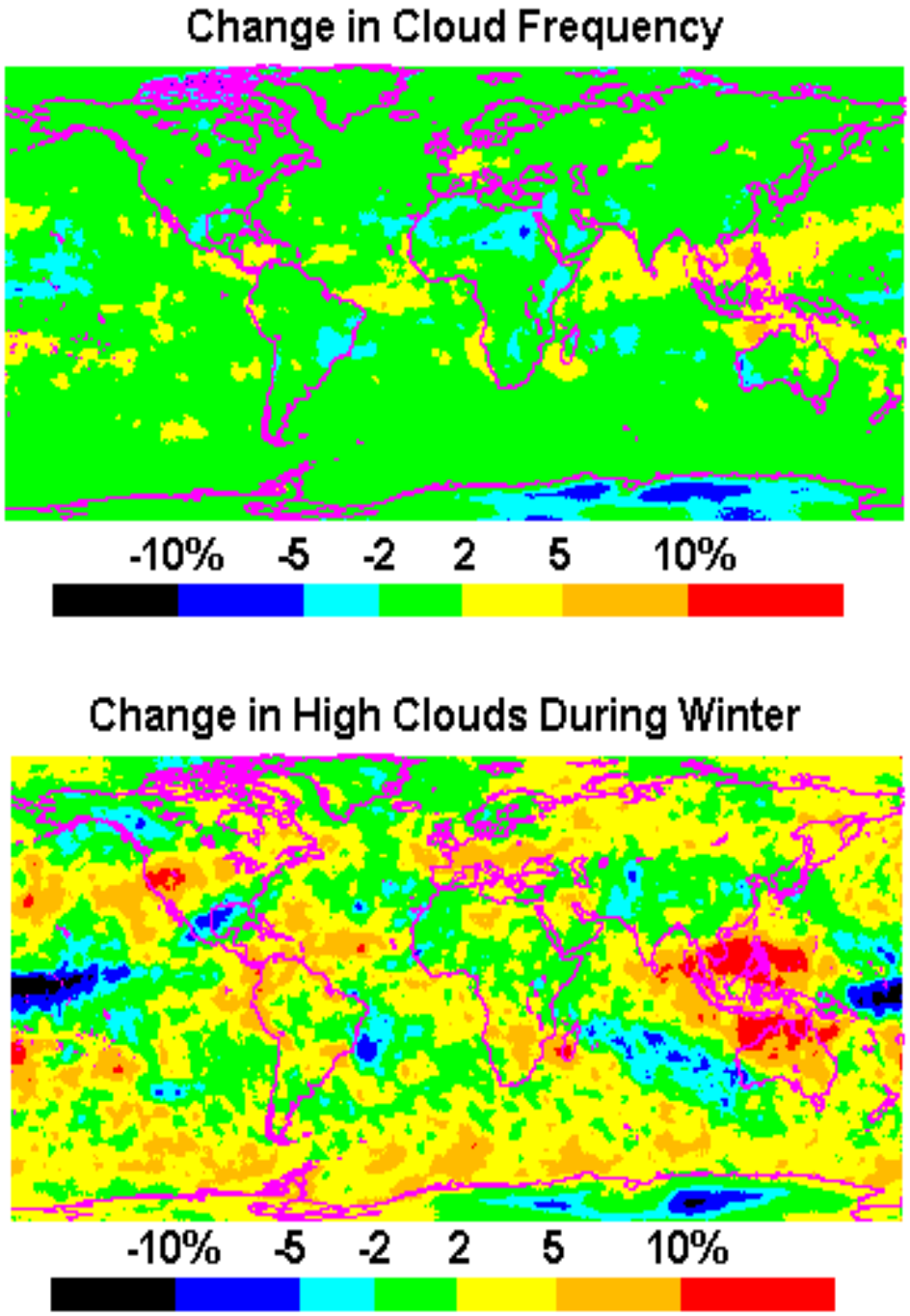

Figure 6.15: The geographical locations of changes in All Cloud (top) and High Cloud (bottom) frequency of detection from the 1980s to the 1990s.

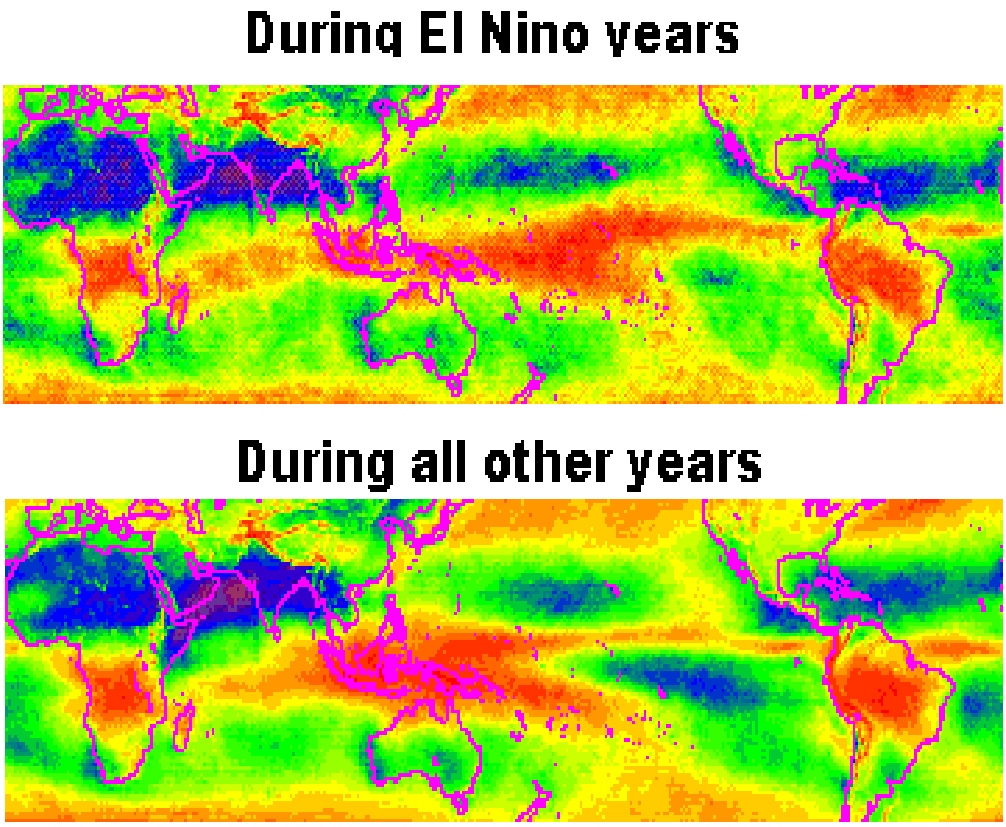

Figure 6.16. High cloud (above 6 km) frequency of detection during El Nino years (top) compared with all the other years (bottom) during northern hemisphere winters (December, January, and February) during the 1980s to the 1990s.